Research Square

Preprints are preliminary reports that have not undergone peer review.
They should not be considered conclusive, used to inform clinical practice,
or referenced by the media as validated information.

Targeting Mosquito Carboxypeptidase B Induces Immediate Metabolic Disruption and Sustained Reduction in Vector Competence

Gaoqian Feng

fenggaoqian@njmu.edu.cn

Nanjing Medical University https://orcid.org/0000-0002-3605-038X

Jian Zheng

Nanjing Medical University

Jinrong Ling

Nanjing Medical University

Qinglong Zhang

Nanjing Medical University

Xinhui Yu

Nanjing Medical University

Zhenyu Rong

Nanjing Medical University https://orcid.org/0009-0006-5872-5719

Yajie Yuan

Nanjing Medical University

Jianxia Tang

Jiangsu Institute of Parasitic Diseases

Stephen Baffour Gyawu

Nanjing Medical University

Jo-Anne Chan

Burnet Institute https://orcid.org/0000-0003-0708-8263

Wenjie Hou

Nanjing Medical University

Yuxuan Lu

Nanjing Medical University

Yonglin Yang

The Affiliated Taizhou People's Hospital of Nanjing Medical University

James Beeson

Burnet Institute

Wenlong Dai

Nanjing Medical University

Jun Cao

Jiangsu Institute of Parasitic Diseases

Article

Keywords:

Posted Date: November 5th, 2026

DOI: https://doi.org/10.21203/rs.3.rs-11487511/v1

License: This work is licensed under a Creative Commons Attribution 4.0 International License.
Read Full License

Additional Declarations: There is **NO** Competing Interest.

Targeting mosquito carboxypeptidase B induces immediate metabolic disruption and sustained reduction in vector competence

Jian Zheng[1, 2, 3, #], Jinrong Lin[1, 3, 4, #], Qinglong Zhang[1, 3, 4], Xinhui Yu[1, 3, 4], Zhenyu Rong[3, 4, 5], Yajie Yuan [1, 3, 4], Jianxia Tang[2], Stephen Baffour Gyawu[1, 3, 4], Jo-Anne Chan[6, 7, 8], Wenjie Hou[1, 3, 4], Yuxuan Lu[1, 3, 4], Yonglin Yang[9], James Beeson[6, 7, 8], Wenlong Dai[3, 4, 5, 10, *], Jun Cao[2, *], Gaoqian Feng[1, 3, 4, 6, *]

[1]NHC Key Laboratory of Antibody Technique, Jiangsu Key Laboratory of Pathogen Biology, Department of Pathogen Biology, Nanjing Medical University, Nanjing, Jiangsu 211166, China

[2]Key Laboratory of National Health Commission on Parasitic Disease Control and Prevention, Key Laboratory of Jiangsu Province on Parasite and Vector Control Technology, Jiangsu Institute of Parasitic Diseases, Wuxi, Jiangsu 214064, China

[3]National Vaccine Innovation Platform, Nanjing Medical University, Nanjing, Jiangsu 211166, China

[4]Nanjing Medical University Taizhou Institute of Pharmaceutical Industry, Taizhou, Jiangsu, China

[5]Department of Pharmaceutics, Nanjing Medical University, Nanjing, Jiangsu 211166, China

[6]Burnet Institute, Melbourne, Australia

[7]Department of Infectious Diseases, University of Melbourne, Australia

[8]Department of Immunology and Department of Microbiology, Monash University, Australia

[9]The Affiliated Taizhou People's Hospital of Nanjing Medical University, Taizhou School of Clinical Medicine, Nanjing Medical University, Taizhou, 225300, China.

[10]Key Laboratory of Immunoregulation and Intervention for Major Chronic Diseases of Jiangsu Province, Nanjing Medical University, Nanjing, Jiangsu 211166, China

[*]Corresponding authors: Gaoqian Feng, Jun Cao and Wenlong Dai, Nanjing Medical University, 101 Longmian Avenue, Nanjing, Jiangsu 211166, China. E-mails: fenggaoqian@njmu.edu.cn (Feng), caojuncn@hotmail.com (Cao) and wenlong.dai@njmu.edu.cn (Dai)

[#]These authors contributed equally to this work.

Abstract: Malaria remains the deadliest mosquito-borne disease. Complementary interventions targeting the vectors are increasingly needed amid insecticide resistance and incomplete intervention coverage. Carboxypeptidase B (CPB), a blood-meal-induced mosquito midgut protease, is a promising transmission-blocking target, but the antibody determinants of protection and the underlying mechanisms remain poorly defined. Here we develop adeno-associated virus vaccines targeting CPB and show that a single immunization induced mosquitocidal and transmission-blocking antibodies in mice. Functional monoclonal antibodies isolated from the immunized mice inhibited CPB enzymatic activity and preferentially recognized the catalytic-pocket region. CPB blockade deprives mosquitoes of essential amino acids, including lysine and arginine, in the midgut. Supplementation of amino-acids substantially rescued the anti-vector and transmission-blocking phenotypes, supporting a causal role for impaired nutrient acquisition. Notably, transmission-blocking activity persisted after vaccine-induced antibodies were no longer detectable in the mosquito, under asynchronous challenge conditions, and was accompanied by persistent depletion of endogenous midgut CPB protein that was not restored by amino-acid supplementation. Together, our findings identified CPB as a functionally vulnerable mosquito antigen and supported a broader principle whereby essential vector physiology can be exploited to simultaneously impair vector fitness and pathogen permissiveness.

INTRODUCTION

Malaria remains a major cause of global morbidity and mortality, posing an ongoing threat to public health. In 2024, an estimated 282 million infections and 610,000 deaths were attributed to malaria, accounting for over 80% of all mosquito-borne disease-related deaths[1,2]. Despite major advances in malaria control, parasite drug resistance and incomplete durability and coverage of existing interventions continue to sustain transmission[3]. Chemical insecticides remain central to vector control, but resistance to multiple commonly used insecticide classes is increasingly widespread among major malaria vectors, including *Anopheles gambiae* and *Anopheles stephensi* (*A. stephensi*)[4-6]. These challenges highlight the need for complementary interventions targeting the parasite-mosquito interface to interrupt parasite transmission or interfere with parasite development within the mosquito vector.

Transmission-blocking vaccines provide an attractive strategy for interrupting malaria transmission by targeting parasite development within the mosquito. The development of

transmission-blocking strategies has primarily focused on antigens from the sexual and mosquito stages of *Plasmodium* parasite[7-11]. An alternative and potentially complementary approach is to target mosquito antigens required for parasite development. The proof-of-concept for this strategy was established nearly two decades ago, when antibodies against the midgut aminopeptidase N (APN) were shown to block *P. falciparum* development within the mosquito[12]. Because these molecules are vector encoded, targeting these antigens is independent of antigenic variation in parasite proteins[13,14]. Moreover, mosquito proteins with essential physiological functions may provide an opportunity to simultaneously impair parasite development and vector fitness. Indeed, malaria transmission mathematical modelling studies indicated a disproportionately large reduction in malaria R_0 upon increasing the mortality among mosquitoes. This underscored the potent epidemiological impact of targeting vector-encoded molecules[15]. Several mosquito midgut proteins have consequently been investigated as transmission-blocking targets[12,16-18]. However, few have been shown to simultaneously affect both parasite development and mosquito reproductive fitness, with carboxypeptidase B (CPB) being one such antigen[18].

CPB is a metalloprotease that is specifically upregulated in mosquitoes upon a blood meal[19,20]. It primarily catalyzes the hydrolysis of basic amino acids from the C-terminus of peptides[21,22], providing essential amino acids for mosquito oogenesis and metabolism[18,20,23]. This function directly links CPB to the reproduction of female mosquitoes and may also indirectly affect *Plasmodium* survival and development by altering the midgut's biochemical microenvironment. Studies by Lavazec et al. and Raz et al. demonstrated that polyclonal antibodies targeting CPB1 in *A. gambiae* and *A. stephensi* blocked CPB enzymatic activity, thereby preventing the sexual development of *P. falciparum* within the anopheline midgut[18,24]. Research on the Malaria Box compounds[25,26] and studies with plant- and leech-derived inhibitors[27] further highlight CPB's importance as a transmission-blocking target. However, despite these proof-of-concept studies, the antibody determinants underlying functional CPB inhibition remain poorly defined, and the physiological mechanisms linking antibody binding to reduced mosquito fitness and impaired *Plasmodium* development have not been fully resolved. Defining these mechanisms is important for translating CPB from a validated mosquito target into a rationally designed transmission-blocking vaccine strategy.

Adeno-associated virus (AAV) vectors are vaccine delivery platforms capable of mediating prolonged transgene expression *in vivo*[28,29] and are therefore capable of inducing durable antibody

responses even after a single administration[30,31]. This characteristic makes AAV vectors ideal for transmission-blocking strategies, in which sustained circulating antibodies are required. AAV-vectored vaccines targeting the *P. falciparum* circumsporozoite protein or Pfs25 have been successfully developed and have demonstrated promising immunoprotective efficacy in proof-of-concept studies[32,33]. Furthermore, the flexible administration route (orally administered) also enables the potential expansion of the application of these transmission-blocking strategies to domestic animals to create a vaccine enhanced zooprophylaxis approach[34], in which domestic animals can be used to divert mosquito bites from humans and deliver the transmission-blocking antibodies to the mosquito vectors.

Here, we developed an AAV-vectored vaccine targeting *A. stephensi* CPB and evaluated its immunogenicity and functional efficacy, with the aims of defining the antibody determinants of protection and resolving the mechanisms underlying its anti-vector and anti-parasite activities.

RESULTS

AAV-CPB vaccination induces CPB-specific antibody responses with distinct clonal architecture

We first investigated whether a single immunization with an adeno-associated virus (AAV) vaccine targeting the mosquito midgut protease carboxypeptidase B (CPB) could simultaneously affect both parasite development and mosquito reproductive fitness, and began by characterizing the antibody response it elicited. The AAV-CPB vaccine was successfully constructed using a well-established AAV vector[35,36]. Integration of the CPB gene was confirmed by PCR and Western blotting (Supplementary Fig. 1A, B). Following either intramuscular (i.m.) or oral (p.o.) immunization of mice, CPB-specific antibody responses were robustly induced in both groups by day 42 post-immunization (Fig 1a, b). Both i.m. and p.o. immunization of the AAV vaccine elicited similar IgG subclass profiles, which were dominated by IgG2b and IgG3 (Supplementary Fig. 1C), with no statistically significant differences between the two routes; the IgG subclass profile induced by the AAV vaccine differed markedly from that induced by the rCPB-Freund's adjuvant control (Fig. 1c). Further characterization of the IgG subclass profile revealed the IgG2a/IgG1 ratio in the i.m. group was significantly lower than that in the rCPB control group (Fig. 1d).

To characterize the antibody repertoire elicited by AAV-CPB vaccination, single B cell BCR sequencing approach was applied to analyze the paired VH and VL sequences that were transcribed

by CPB specific B cells. Among the 28 successfully retrieved antibody clonotypes, IGHV1 family genes were preferentially represented, with IGHV1-62-2*01, IGHV1-18*04 and IGHV1-47-8*01 the most frequently used VH genes. Further analysis of the clonotypes identified 5 expanded clonal families comprising 21 of the 28 antibody sequences, together with 7 singleton clonotypes (Fig. 1e). The largest clonal family comprised 9 antibody sequences sharing IGHV1-62-2*01/IGHJ4*01 usage (Supplementary Table 2). The somatic hypermutations were detected in both heavy- and light-chain variable regions (ranging from 0% to 4.50% and from 0% to 4.65%, respectively), with the highest heavy-chain frequency observed in singleton B7 (4.50%) and the highest light-chain frequencies in the clonally related functional clones E8 and D8 (4.65%) (Supplementary Fig. 2). Together, these findings demonstrate a clonally structured CPB-specific antibody response with evidence of vaccine-induced somatic diversification.

The AAV-CPB vaccine confers mosquitocidal and transmission-blocking activity against Plasmodium berghei parasites

To determine the mosquitocidal efficacy of the AAV-CPB vaccines, mice that had received the AAV-CPB vaccines were used to provide blood meals to *A. stephensi* mosquitoes (Fig. 2a). Blood meals from the vaccine-immunized mice drastically shortened mosquito lifespan, reducing mean survival times to 8.20 days (i.m.) and 6.69 days (p.o.), compared with 9.89 days for controls and 6.36 days for the rCPB-Freund adjuvant group over the 11-day observation period (all $P < 0.01$ versus control; Fig. 2b). The mosquitoes fed on AAV-CPB-immunized mice also produced fewer eggs, with the p.o. group exhibiting the most pronounced reduction. Notably, the oviposition rate in the mock-vaccine group was 73.7%, whereas it dropped to 40.0% in the i.m. group and to 37.8% in the p.o. group ($P = 0.0027$, $P = 0.0018$ respectively; Fig. 2c).

To evaluate the vaccine-induced transmission-blocking activity, the immunized mice were infected with *Pb*-GFP before being fed on by the *A. stephensi* mosquitoes (Fig. 2d). Mosquitoes fed on AAV-CPB-immunized mice carried significantly fewer oocysts than those fed on control mice, with significant reductions observed in both the i.m. and p.o. groups ($P = 0.0171$ and $P = 0.0198$, respectively; Fig. 2e, f). Collectively, these results demonstrate that the AAV-CPB vaccine confers both mosquitocidal and transmission-blocking effects.

To confirm that antibodies were the primary factor of the vaccine-induced outcome, purified CPB-specific polyclonal antibody (CPB-pAb) from AAV-CPB immunized mice were tested in membrane feeding assays. These antibodies demonstrated potent mosquitocidal and fecundity-

inhibition activities (P = 0.0001 and P = 0.003, respectively; Supplementary Fig. 3A-C). Passive transfer of these antibodies to *Pb*-GFP infected mice also blocked transmission of the parasites to mosquitoes as indicated by reduced oocyst development (P = 0.0113) and reduced infection rate in the mosquitoes (from 69.8% to 30.0%, P = 0.0004; Supplementary Fig. 3D-G). Moreover, the vaccine-induced antibodies cross-reacted with proteins from *Aedes aegypti*, *Anopheles sinensis* and *Culex pipiens pallens*, suggesting potential cross-reactivity across multiple mosquito species (Supplementary Fig. 4).

Epitope-specific antibodies targeting the CPB active site correlate with transmission-blocking activity

Not all vaccine-induced antibodies are equal. Having established that CPB-directed immunity is functional at the polyclonal level, we next investigated which antibody clones actually mediated protection, including the epitope features that distinguished them. We therefore recombinantly expressed three representative monoclonal antibodies isolated from CPB-specific single B cells of immunized mice (mAbE8, mAbC8 and mAbD8; Supplementary Table 2) and compared their activities in parallel. Among the monoclonal antibodies, mAbE8 and mAbD8 exhibited marked mosquitocidal effects (Fig. 3a) and reduced mosquito oviposition by decreasing the oviposition rates from 72.2% in the control group to 47.6% in the mAbE8 group and 56.0% in the mAbD8 group, respectively (P = 0.038 and P = 0.274, respectively; Fig. 3b). Consistent with these findings, mAbE8 and mAbD8 significantly inhibited *Plasmodium* transmission to the mosquitoes when the antibodies were passively transferred to *Pb*-GFP infected mice. In contrast, no mosquitocidal or transmission-blocking effects were observed for mAbC8, underscoring the epitope specificity of CPB-directed protective immunity (Fig. 3c, d).

Previously published results have suggested that CPB specific antibodies exerted mosquitocidal and transmission-blocking activity by inhibiting the enzymatic activities of CPB [18,24]. To directly test whether the differential functional activities of mAbE8, mAbC8, and mAbD8 could be attributed to their distinct capacities to inhibit CPB catalysis, we assessed their effects on CPB enzymatic activity *in vitro*. Indirect ELISA confirmed that all three monoclonal antibodies bound to immobilized CPB, with mAbC8 displaying the strongest binding reactivity (Supplementary Fig. 5A). However, enzymatic kinetic assays revealed that mAbE8 and mAbD8 profoundly inhibited CPB catalytic activity, reducing hippuric acid production to near-background levels, whereas mAbC8 had minimal impact on substrate hydrolysis (Supplementary Fig. 5B). Quantification of

specific activity during the linear reaction phase demonstrated that CPB alone exhibited robust enzymatic activity (119.4 ± 7.6 U/mg). In contrast, mAbE8 and mAbD8 treatment resulted in drastic inhibition (8.2 ± 14.3 U/mg and 16.5 ± 19.2 U/mg, respectively; $P = 0.0038$ and $P = 0.0084$ versus CPB alone, respectively), while mAbC8 failed to significantly suppress CPB activity (93.2 ± 47.9 U/mg; $P = 0.6695$) (Supplementary Fig. 5C). Collectively, these results established that the protective efficacy of mAbE8 and mAbD8 correlated with their capacity to inhibit CPB enzymatic activity, whereas the non-neutralizing mAbC8, despite its strong antigen-binding capacity, does not block CPB catalytic function.

Given the marked functional divergence among mAbE8, mAbD8 and mAbC8 in their mosquitocidal and transmission-blocking activities despite their comparable binding activities, we asked whether these differences could be attributed to their distinct binding epitopes. To dissect the structural basis for this functional divergence, structural modeling using AF3 was performed to explore the binding epitopes of these mAbs. The mAbE8 and mAbD8 were predicted to bind the rim and entrance of the enzymatic pocket of CPB, contacting pocket-lining residues that form the substrate-binding cleft. This binding mode positions the antibodies to sterically occlude access to the catalytic core residues [27]. In contrast, mAbC8 bound to a distal, non-functional surface region of the protein distant from the catalytic pocket (Fig. 3e). These findings suggest that antibodies targeting the CPB enzymatic pocket, rather than those with merely high binding reactivity, are required for effective mosquitocidal and transmission-blocking activity.

The predicted binding footprints were supported by NH_4SCN dissociation analysis of alanine-scanning mutants. For mAbE8, substitutions at Arg^{32}, Glu^{34}, Arg^{36}, Glu^{37}, Arg^{62}, Gly^{311}, Glu^{329}, Glu^{349}, Glu^{351} and Asp^{357} significantly reduced avidity, with the Glu^{351} Ala mutant showing the strongest disruption with avidity index around 0.25. mAbD8 displayed a similar sensitivity pattern centered on the same N-terminal cluster. Avidity was reduced by substitutions at Arg^{32}, Glu^{34}, Leu^{60}, Asp^{84} and Glu^{349}, whereas no detectable effect was observed for substitutions at Arg^{36}, Gly^{61}, Arg^{62} and Asn^{63}. Notably, Arg^{32}/Glu^{34}/Glu^{349} formed a shared epitope core that was required by both neutralizing mAbs. In contrast, binding of mAbC8 was dependent on a distinct and limited residue set: avidity was reduced by the Glu^{329} and Thr^{418} substitutions, while no disruptive effect was detected for the Arg^{333} substitution. Together, these data indicated that the two protective mAbs engaged overlapping epitopes located in the vicinity of the CPB catalytic pocket, whereas

mAbC8 recognized a separate region, in full agreement with the structural modeling predictions (Fig. 3f).

Having established that mAbE8 and mAbD8 recognize a functional catalytic-pocket-associated epitope whereas mAbC8 did not, we asked whether this difference was related to their clonal origins. Sequence analysis revealed distinct clonal origins among the three mAbs: mAbE8 and mAbD8 were clonally related, sharing identical heavy chain germline gene and CDR3 sequences, whereas mAbC8 belonged to a separate lineage (Supplementary Table 2). This observation prompted us to ask whether catalytic-pocket recognition was preferentially associated with particular clonotypes within the broader vaccine-induced CPB-specific repertoire. We further extended the structural analysis to all 28 clonotypes. Nine clonotypes whose CDRs were predicted to reside within 8 Å of the pocket were classified as active site-targeting (AST) clonotypes, while the remaining 19 clonotypes were classified as non-active-site (non-AST) clonotypes (Supplementary Fig. 6A, Supplementary Table 3). An uneven distribution of the AST clonotypes was found among the clonal families, with enrichment in Fam.2 and Fam.5 (Fig. 3g, Supplementary Fig. 6B, C). Notably, the experimentally characterized mAbE8 and mAbD8 were correctly classified as AST, while mAbC8 was classified as non-AST, consistent with their experimentally defined functional phenotypes. Together, these findings suggest that catalytic-pocket recognition is associated with selected clonal backgrounds within the vaccine-induced CPB-specific antibody repertoire.

Vaccine-induced antibodies targeting CPB deprive mosquitoes and malaria parasites of essential amino acids

Building on the previous finding that polyclonal antibodies block the enzymatic activity of CPB to prevent *P. falciparum* sexual development in the mosquito midgut[18,24], and that AAV-CPB induced functional mAbs bind to the enzymatic pocket of CPB, we asked whether this effect was mediated through perturbation of amino acid metabolism. We performed targeted amino acid metabolomic analysis on *Anopheles* midguts at 24 hours post-blood meal (PBM) following the vaccine-induced CPB-pAb intervention. Principal component analysis revealed a complete separation between the CPB-pAb treated and control groups along PC1, indicating profound antibody-induced metabolic perturbation (Supplementary Fig. 7A). Volcano plot analysis identified 30 differentially abundant metabolites (18 upregulated and 12 downregulated) among 127 targeted species (Supplementary Fig. 7B), suggesting that anti-CPB antibodies exert highly

specific rather than broadly toxic effects on amino acid metabolism. Consistent with the established role of CPB in blood protein digestion, both of its canonical C-terminal substrates were significantly reduced in the CPB-pAb group: lysine ($P = 0.0062$) and arginine ($P = 0.0117$) (Fig. 4a). Along with these two direct substrates, methionine, asparagine, glycine and serine were also significantly reduced, whereas alanine and tyrosine showed consistent downward trends; in contrast, all other measured amino acids, including aspartic acid, glutamic acid and glutamine, remained unaffected (Supplementary Fig. 7C). This pattern supports a specific defect in CPB-mediated terminal digestion rather than a generalized impairment of amino acid digestion, and points to lysine and arginine deprivation as the most direct metabolic consequence of CPB inhibition. We therefore selected these two CPB substrates for functional validation in subsequent experiments.

C-terminal lysine and arginine were identified as specific substrates for CPB in previous studies[37]. Therefore, to test whether depletion of these metabolites underlies the mosquitocidal and transmission-blocking effects, we supplemented blood meals with exogenous lysine and arginine during membrane feeding assays using vaccine-induced anti-CPB antibodies. Remarkably, supplementation with these amino acids significantly reversed both the mosquitocidal activity and the fecundity inhibition induced by CPB-pAb (Fig. 4c, d). To test whether lysine and arginine supplementation could rescue the transmission-blocking effects of CPB *in vivo*, *Pb*-GFP infected mice were passively immunized with CPB-pAb and supplemented with both amino acids prior to mosquito feeding (Fig. 4e, f). The transmission-blocking effect of CPB-pAb was similarly abrogated upon lysine and arginine supplementation. This mechanism was further validated using monoclonal antibodies, *Pb*-GFP infection of the mosquitoes in the presence of mAbE8 and mAbD8 was fully restored upon supplementation with lysine and arginine. This result indicated that the activity of these functional antibodies relies on inhibiting CPB-mediated liberation of these specific amino acids. In contrast, mAbC8, which binds CPB with comparable binding reactivity yet lacks transmission-blocking activity, was unaffected by lysine and arginine supplementation (Fig. 4g, h).

Collectively, these results indicate that the mosquitocidal and transmission-blocking activities elicited by the AAV-CPB vaccine rely on the recognition and blockade of CPB enzymatic activity, which deprives mosquitoes and *Plasmodium* parasites of the critical amino acids required for metabolism and oogenesis.

AAV-CPB immunization induced sustained transmission-blocking under asynchronous challenge

Given the delivery of vaccine-induced mosquitocidal antibodies may not be simultaneous with the transmission of *Plasmodium* to mosquitoes in field settings, we further assessed the transmission-blocking efficacy of the AAV-CPB vaccine under asynchronous conditions. The mosquitoes were challenged with *Pb*-GFP after the full digestion of the initial blood meal from the AAV-CPB vaccine immunized mice (Fig. 5a). Notably, even when the infection challenge was performed days after the initial blood meal, significantly fewer oocysts were observed in the AAV-CPB vaccine group compared to the control group (Fig. 5b, c). We next performed a reciprocal experiment, in which mosquitoes were initially infected with *Pb*-GFP and, after oviposition, received a secondary blood meal from AAV-CPB-immunized mice (Fig. 5d). Remarkably, even when antibody exposure occurred after the initial infection, a significant reduction in oocyst number was observed in the AAV-CPB vaccine group compared to the controls (Fig. 5e, f).

Sustained transmission-blocking was correlated with antibody-mediated disruption of endogenous CPB homeostasis

To determine whether the same antibody neutralization mechanism underlies the sustained protection observed beyond the initial blood meal, we first examined the requirement for antibodies in this long-lasting effect using passive immunization. Mosquitoes fed on mice passively immunized with vaccine-induced CPB-pAb carried significantly fewer oocysts even when the parasite challenge was performed on day 3 post the initial blood meal (Fig. 6a-f) suggesting a critical role for antibodies for sustained transmission-blocking activity. However, immunohistochemistry (IHC) and Western blotting (WB) analyses revealed that CPB-pAb were no longer detectable in mosquitoes beyond 3 days post the initial antibody-spiked blood meal (Fig. 6g, h) suggesting additional mechanisms were involved beyond direct antibody binding to CPB. Therefore, we investigated if CPB was affected by antibody intervention. Under physiological conditions, the endogenous CPB is a midgut-specific digestive enzyme and predominantly expressed in the midgut compared to other mosquito tissues (Supplementary Fig. 8A). The secreted CPB was localized to the interior side of the midgut (Supplementary Fig. 8B). The transcription of *cpb* rapidly increased upon ingestion of a blood meal (Supplementary Fig. 8C). Importantly, *cpb* transcription levels continued to rise in *Plasmodium*-infected mosquitoes beyond 24 hours and

remained elevated at 96 hours, 7 days, and 14 days post-infection (Supplementary Fig. 8D). A strong positive correlation was observed between *cpb* transcription and parasite load (Fig. 6i), suggesting that CPB is a key contributor for the development of *Plasmodium* oocyst in the mosquito.

Given that antibodies were no longer detectable beyond 3 days whereas transmission-blocking persisted for days, we next examined the expression of endogenous *cpb* following transient CPB-pAb exposure. On day 3 post blood meal, mosquitoes exposed to CPB-pAb displayed a markedly higher level of *cpb* transcription compared with controls (P = 0.0332 versus control). Supplementation of lysine and arginine significantly reduced *cpb* transcription relative to CPB-pAb treatment alone (P = 0.0238), restoring *cpb* transcription levels towards those of the baseline levels (Fig. 6j). In contrast, the abundance of CPB protein within the midgut epithelium remained significantly reduced in both the CPB-pAb group and the CPB-pAb+AAs group (P = 0.009 and P = 0.001 versus control, respectively), and was significantly lower in the CPB-pAb+AAs group than in the CPB-pAb group alone (P = 0.0311; Fig. 6k, l). Thus, amino-acid supplementation altered the transcriptional response to CPB-pAb exposure but did not restore intracellular CPB protein abundance, revealing a dissociation between *cpb* transcript and protein levels.

DISCUSSION

The concept of targeting mosquito molecules required for both vector physiology and parasite development has been previously explored with antigens including *Anopheline* alanyl APN[38]. However, APN and other mosquito-derived candidates, including fibrinogen-related protein 1 and serine protease inhibitors, lack the direct mosquitocidal activities[12,16,17,38]. By contrast, CPB targeting imposes two complementary barriers to transmission, including reducing vector fitness through impaired blood meal utilization and a less permissive midgut environment for *Plasmodium* sexual development. This distinction is critical because parasite-targeting TBVs are inherently constrained by antigen polymorphism, stage-specific expression windows, and the inability to directly suppress vector populations[7-9]. A vector-derived target such as CPB circumvents these limitations by avoiding direct dependence on parasite antigen sequence variation, while the observed cross-reactivity of CPB-pAb with proteins from other mosquito species[24] raises the possibility that conserved digestive enzymes may support broader, multi-species vector-targeted interventions.

Our monoclonal antibody analysis revealed a marked dissociation between antigen binding and functional efficacy. Despite exhibiting comparable CPB-binding reactivity, only mAbE8 and mAbD8 conferred potent mosquitocidal and transmission-blocking effects, whereas mAbC8 remained functionally inactive, indicating that antibody binding alone is insufficient for protection. This finding aligns with structural vaccinology studies of Pfs25 and Pfs48/45, which demonstrated that antibody binding alone is insufficient for transmission-blocking activity and that recognition of specific conformational epitopes is required[39,40]. In our study, the functional importance of the CPB enzymatic pocket provided a mechanistic explanation for this divergence as mAbE8 and mAbD8 inhibited CPB enzymatic activity and were predicted to recognize the catalytic-pocket region, where mAbC8 recognized a distinct non-functional surface with no inhibition of CPB enzymatic activity. The clonal relationships of the functional mAbE8 and mAbD8, together with the enrichment of predicted AST antibodies within the selected clonal families, further suggested that functionally relevant epitope recognition is associated with particular antibody clonotypes within the vaccine-induced repertoire. This epitope function relationship has direct implications for next-generation CPB based immunogen design, suggesting that structure-guided engineering to preferentially expose or stabilize the enzymatic pocket region may help focus antibody responses towards functional vulnerable epitopes.

Mechanistically, the functional importance of CPB in post-blood-meal protein digestion provided a clear hypothesis that antibody-mediated interference with CPB activity could restrict the availability of amino acids required for mosquito metabolism and reproduction. Our targeted metabolomic analysis confirmed the profound perturbation of amino acid availability following CPB-antibody treatment. This metabolic reprogramming positions CPB as a critical "nutritional gatekeeper" at the vector-parasite interface. Recent evidence has established that *Plasmodium* sporogonic development is exquisitely sensitive to the mosquito's metabolic status. Lampe et al. demonstrated that miR-276-mediated regulation of branched-chain amino acid catabolism through branched-chain amino acid transferase (BCAT) directly determines both mosquito fecundity and parasite sporozoite production[23]. In this regulatory hierarchy, CPB functions as the upstream proteolytic valve controlling the initial liberation of free amino acids from ingested blood proteins. Lysine and arginine were reported as the canonical C-terminal substrates of CPB[14,23]. The marked reduction in amino acid levels, particularly of the two CPB substrates, indicates that CPB blockade generated a nutrient-limited midgut environment. Beyond these two substrates, broader evidence

indicates that *Plasmodium* sexual stages exhibit stage-specific metabolic dependencies on host-derived amino acids: for example, glutamine, which was not among the metabolites altered in our dataset, has been shown to serve as a major carbon source for the parasite TCA cycle during oocyst development[41]. Importantly, we showed supplementation of blood meals with exogenous lysine and arginine substantially reversed both the mosquitocidal and fecundity-impairment effects of the CPB-specific antibodies and attenuated the transmission-blocking effect. This functional rescue provided strong evidence for a causal role of nutrient deprivation in the anti-vector and anti-parasite phenotypes. The observation that amino acid supplementation restored *P. berghei* infectivity suppressed by functional mAbE8 and mAbD8 further confirms that the transmission-blocking activity of these antibodies is mechanistically linked to CPB enzymatic inhibition.

Beyond this immediate metabolic effect, we found that transmission-blocking activity persisted for days after vaccine-induced CPB-pAb had become undetectable in the mosquito (Figs. 5, 6g, h). This challenges the prevailing view that sustained high-level antibody concentrations in the mosquito are required for transmission-blocking immunity[7-9]. Such lasting refractory states are not without precedent in *Anopheles*, where a single immune priming exposure induces protection that persists for weeks[42-44]. Our data indicated that transient CPB antibody engagement similarly established persistent CPB protein depletion in the midgut that was not reversed by amino-acid supplementation. The molecular basis of this state is a dissociation between *cpb* transcript and CPB protein. Antibody-exposed mosquitoes mounted a compensatory *cpb* transcriptional response at day 3 that was abolished by amino-acid supplementation, showing that this response is driven by amino-acid deprivation through a nutrient-feedback mechanism[45]. Nevertheless, the level of intracellular CPB protein remained low at the same time point and was further reduced by amino-acid supplementation. These findings suggest that antibody-mediated CPB inhibition triggers both an acute nutrient-responsive transcriptional response and a longer-lasting alteration in CPB protein homeostasis. The latter cannot be explained simply by reduced *cpb* transcription or continued amino-acid deprivation and may involve regulation of CPB translation, stability, processing, or trafficking. Whether this persistent protein-level alteration directly mediates the sustained reduction in vector competence remains to be determined.

The practical implementation of this strategy depends critically on a vaccine platform capable of maintaining sufficient circulating antibody titers for uptake during mosquito blood feeding. This requirement highlights a major limitation of current protein-based TBVs: clinical trials of Pfs25-

EPA and Pfs230D1-EPA have shown that functional transmission-blocking antibody activity requires multiple vaccinations (up to four doses) and declines rapidly after the final immunization[7-9]. AAV vectors are particularly attractive in this context because they function as *in vivo* antigen factories, supporting prolonged transgene expression and durable humoral immunity for months to years following a single administration[30,31]. Consistent with this rationale, AAV-CPB vaccination elicited robust CPB-specific antibody responses following both i.m. and p.o. administration. The ability to induce functional responses through oral delivery is especially notable, as it raises the possibility of implementing this strategy through bait-based or feed-based immunization of domestic animals. The distinct IgG subclass profile elicited by AAV-CPB further suggests that the vaccine platform and administration route influence the qualitative composition of the antibody response, although the functional significance of these subclass differences remains to be determined.

The observation that transmission-blocking activity can extend beyond the antibody-containing blood meal may further increase the practical value of this strategy by reducing the dependence on exact temporal coincidence between antibody uptake and parasite acquisition. These properties raise the possibility of extending CPB vaccination to domestic animals as part of a zooprophylaxis-based approach, whereby blood feeding on an immunized host could simultaneously expose mosquitoes to anti-vector and transmission-blocking antibodies. Unlike conventional zooprophylaxis approaches, which primarily divert mosquito feeding from humans to animals[46], vaccination of animal hosts could potentially convert such blood meals into an intervention that reduces both mosquito fitness and subsequent vector competence. The potential impact of such modest reductions in oocyst burden is substantial: recent quantitative analyses demonstrate a strong, highly significant correlation between mosquito parasite burden and the efficiency of onward transmission, such that even partial suppression of parasite loads could disproportionately reduce human infection outcomes[15,47]. However, proof-of-concept studies in large animal models are required to establish the immunogenicity, durability, dosing requirements, and protective efficacy of AAV-CPB vaccination in potential target hosts under field-relevant conditions.

Nevertheless, several questions remain. The causal relationship between antibody-induced CPB downregulation and the persistent reduction in vector competence must be formally established through genetic rescue experiments, specifically, by restoring CPB expression or activity in antibody-exposed mosquitoes and determining whether this abrogates the sustained transmission-

blocking phenotype. The structural basis for the functional divergence between mAbE8/mAbD8 and mAbC8 should be resolved through crystallographic or cryo-EM analysis of antibody-CPB complexes, which would enable rational immunogen design to focus the antibody response on protective enzymatic-pocket epitopes. The functional mosquitocidal and transmission-blocking activity of anti-CPB antibodies must be validated across additional vector species, including *Anopheles funestus* and *A. gambiae*, to assess the breadth of protection afforded by conserved CPB epitopes[24]. The differential IgG subclass profiles and their potential contributions to complement-dependent mosquito impairment require further investigation to optimize the vector and route of immunization. Finally, extension beyond the current mouse model will require evaluation of the magnitude, durability, and functional quality of CPB-specific antibody responses in intended domestic animal hosts, as well as field-relevant delivery strategies and cost-effectiveness analyses.

In summary, our findings established CPB as a functionally vulnerable mosquito antigen through which vaccine-induced antibodies can simultaneously impair vector fitness and *Plasmodium* development by creating an amino acid-deprived midgut environment. The identification of enzymatic-pocket-dependent antibody activity, together with evidence that transient antibody exposure can produce sustained effects extending beyond detectable antibody persistence, broadens the mechanistic basis by which mosquito-targeted vaccines may suppress malaria transmission. More broadly, this study provides a conceptual framework for developing vector-targeted vaccines that exploit essential mosquito physiology to combine anti-vector and anti-parasite activity within a single transmission-blocking intervention.

MATERIALS AND METHODS

Sources of Anopheles stephensi, Plasmodium and Experimental Animals

The *A. stephensi* mosquitoes were obtained from the Jiangsu Institute of Parasitic Diseases (Wuxi, China) and maintained in an insectary at 26 ± 1°C, 80 ± 5% relative humidity, under a 12-hour light/12-hour dark cycle at a light intensity of 2,000 lumens. Larvae were fed a formulated diet consisting of porcine liver powder, yeast powder, and commercial fish feed (TetraMin, Tetra, Germany). Adult mosquitoes were provided with 10% (w/v) glucose solution ad libitum and maintained on a 12-hour light/dark cycle. For routine blood feeding, 6- to 8-week-old female BALB/c mice were anesthetized with isoflurane and exposed to mosquito cages for 1 hour twice per week. Only fully engorged females were used in subsequent experiments.

The *Plasmodium berghei* ANKA strain expressing GFP-luciferase (*Pb*-GFP, kindly provided by Prof. Ian Cockburn, Australian National University [48]) was used for all transmission-blocking assays. Cryopreserved *Pb*-GFP infected erythrocytes were thawed in 3% (w/v) NaCl and immediately injected intravenously into recipient BALB/c mice (1×10^6 infected red blood cells per mouse). Parasitemia and gametocytemia were monitored daily by Giemsa-stained thin blood smears. Mosquito infections were performed on day 3 post-infection when gametocytemia reached optimal levels (typically >0.5% of total erythrocytes).

All animal experiments were conducted using specific pathogen-free female BALB/c mice (6 weeks old, 18-22 g) obtained from the Experimental Animal Center of Nanjing Medical University. Animals were housed in individually ventilated cages under standard conditions (22 ± 2°C, 55 ± 10% humidity, 12-hour light/dark cycle) with free access to standard chow and water. All procedures were approved by the Institutional Animal Care and Use Committee of Nanjing Medical University (approval no. IACUC-2308016).

Packaging and purification of the AAV Vector Vaccines

The AAV-CPB are AAV1 and AAV6 encapsidated vaccine vectors with the self-complementary double strand AAV genome expressing carboxypeptidase B protein. For AAV packing plasmids pscAAV-CMV-CPB preparation, codon optimized *cpb* gene was inserted under the control of CMV promoter and carries a short SV40 polyadenylation signal (poly-A). Small-scale vector preparations were generated as previously described by Zabaleta et al. [30] with some modification. Briefly, triple transfection of AAV1-CPB and AAV6-CPB, ITR-flanked transgene pscAAV-CMV-CPB, pAAV1 or pAAV6 (AAV2 rep followed by AAV1 or AAV6 capsid), and pALD-X80 adenoviral helper plasmids by polyethylenimine (PEI) (Polysciences, cat. no.24765-2) in a 1:1:1 ratio, respectively, into HEK293 cells in 150 cm^2 dish using a PEI/DNA ratio of 5:1 (w/w). Three days after transfection, vectors were harvested and purified by AAV-max® Ultra Purification Kit (Denovec, cat. no. DTK2501). AAV titers were determined using the AAV-max® Ultra-Sensitive Titer Kit (Denovec, cat. no. DTK2502).

Recombinant CPB Protein Expression

The coding sequence of *A. stephensi* CPB was cloned into the pcDNA3.4 vector and expressed in Expi293F cells (Thermo Fisher Scientific, cat. no. A14527). Culture supernatants were harvested 5 days post-transfection, and the recombinant His-tagged CPB protein was purified under native

conditions using Ni-NTA affinity chromatography, followed by buffer exchange into PBS via dialysis. Protein integrity and purity were confirmed by SDS-PAGE (~50 kDa).

Mouse Immunization protocols and isolation of mouse polyclonal IgG

Mice were randomly assigned to three immunization groups including AAV-i.m. group, in which mice received a single dose of 1×10^{11} vector genomes of AAV1-CPB in 50 μL PBS, divided equally into both quadriceps femoris muscles; AAV-p.o. group, in which mice received 1×10^{11} vector genomes of AAV6-CPB in 200 μL PBS by oral gavage; recombinant protein control group, in which mice were immunized subcutaneously with 50 μg rCPB emulsified in complete Freund's adjuvant for priming, followed by two booster doses (25 μg each) with incomplete Freund's adjuvant at 21-day intervals to provide a benchmark for conventional protein-adjuvant vaccination. The negative control mice received PBS via the corresponding routes. Sera were collected at baseline and at indicated time points post-immunization.

CPB-pAb was purified from pooled sera of AAV-CPB-immunized mice using Protein A/G affinity chromatography using method described in the user manual (HiTrap Protein A/G HP, Cytiva). The eluted IgG was immediately neutralized and dialyzed against PBS. The IgG concentration was adjusted to 10 mg/mL and stored at -80°C. Naïve mouse IgG was purified from immune naïve mice and served as a negative control. Antigen-specific titers were determined by ELISA against rCPB.

Membrane feeding assays (MFA) and evaluation of mosquitocidal activity

Newly emerged adult female *A. stephensi* mosquitoes were maintained under standard insectary conditions and starved for 24 hours prior to feeding. For polyclonal antibody MFA, fresh mouse blood was collected by cardiac puncture into heparin-coated tubes (BD, cat. no. 367874) and immediately mixed with purified CPB-specific mouse IgG or naïve mouse IgG at a final concentration of 1 mg/mL (unless otherwise specified). For monoclonal antibody MFA, purified mAbE8, mAbC8, mAbD8, or control mouse IgG (Sigma-Aldrich, cat. no. I5381) was added to defibrinated mouse blood at a final concentration of 400 μg/mL. Blood mixtures (500 μL) were loaded into a glass membrane feeder covered with Parafilm M (Bemis, cat. no. PM996) and maintained at 37°C by a circulating water bath. Mosquitoes were allowed to feed for 1 hour in the dark. Fully engorged females were briefly anesthetized at 4°C, counted, and transferred individually to 50-mL conical tubes covered with mesh lids. Mosquitoes were maintained at 26 ±

1°C with 10% glucose solution ad libitum. An oviposition substrate (ultrapure water in a 10-cm diameter petri dish lined with Whatman filter paper) was provided at 24 hours PBM. Mosquito survival was monitored daily for 11 days. Dead mosquitoes were recorded and removed. At 72 hours PBM, the surviving females were transferred to individual oviposition cups, and eggs were counted under a dissecting microscope (Olympus SZX7) at 96 hours PBM. Oviposition rate was calculated as the percentage of blood-fed females that laid at least one egg.

Transmission-blocking assays using Plasmodium berghei infected mice

For direct feeding transmission-blocking assays, BALB/c mice were first immunized with AAV-CPB vectors or control PBS as described above. On day 42 post-immunization, mice were intravenously infected with 1×10^6 *Pb*-GFP infected erythrocytes. On day 3 post-infection, when optimal gametocytemia was achieved, mice were anesthetized with isoflurane and placed individually into mosquito cages containing approximately 50 starved female *A. stephensi* mosquitoes for 1 hour. After feeding, mice were removed and returned to their home cages. Blood-fed mosquitoes were maintained at 21°C on 10% glucose solution supplemented with 0.2% (w/v) p-aminobenzoic acid (PABA; Sigma-Aldrich, cat. no. A9878). On day 14 PBM, mosquito midguts were dissected in PBS under a fluorescence stereomicroscope, and oocysts were visualized by GFP fluorescence using an Olympus BX53 microscope equipped with a UPlanSApo 10×/0.40 objective and a DP74 camera. Oocyst numbers per midgut were counted manually. The prevalence of infection was defined as the percentage of mosquitoes harboring at least one oocyst. Infection intensity was defined as the average number of oocysts per midgut.

For transmission-blocking assays using passively immunized mice, mice infected with *Pb*-GFP received 100 μL of CPB-specific polyclonal mouse IgG or naïve mouse IgG (10 mg/mL in PBS) via tail vein injection on day 3 post-infection. Control mice received 100 μL PBS. At 15 min post-transfer, mice were exposed to mosquitoes for blood feeding, and subsequently handled in the same way described above.

Asynchronous transmission-blocking assays

Two asynchronous challenge experiment designs were employed to evaluate sustained transmission-blocking activity independent of direct antibody persistence.

Design 1: Antibody-first challenge. Mosquitoes were allowed to feed on uninfected mice that had been immunized with AAV-CPB (p.o.), rCPB-s.c. or PBS mice (day 0). Following complete blood

meal digestion and oviposition, mosquitoes were challenged with a second blood meal from *Pb*-GFP infected mice (day 3). Mosquito midguts were dissected on day 17 post-initial blood meal for oocyst enumeration.

Design 2: Parasite-first challenge. Mosquitoes were first fed on *Pb*-GFP infected mice (day 0), allowed to complete digestion and oviposition, and then fed on AAV-CPB (p.o.), rCPB-s.c. or PBS immunized uninfected mice (day 3). Midguts were dissected on day 14 post-initial infection for oocyst enumeration.

For polyclonal antibody asynchronous assays, mice were passively immunized with 100 μL CPB-specific mouse IgG (10 mg/mL) or naïve mouse IgG via tail vein injection. Mosquitoes fed on these mice for the initial blood meal, followed by the reciprocal challenge 3 days later as described above.

Single B cell sorting and antibody cloning

The spleens were harvested from AAV-CPB immunized mice 42 days post-immunization and dissociated mechanically into single-cell suspensions, followed by erythrocyte lysis. Antigen specific single B cell sorting was performed using methods adopted from previous publication[49]. Briefly, cells were stained with the following fluorophore-conjugated antibodies: CD138-PE, CD38-PE/Cy7, CD93-APC, B220-BV421, and IgD-BV510, together with FITC-conjugated rCPB (prepared using the FITC labeling kit, Sigma-Aldrich, cat. no. RPN7102), which served as a fluorescent bait antigen to identify CPB-reactive B cells. Single CPB-reactive B cells were sorted into 96-well PCR plates containing lysis buffer using a BD FACSAria III cell sorter. Plates were sealed and stored at -80°C immediately after sorting until reverse transcription.

Antibody heavy chain (VH) and light chain (VL) variable region sequences were amplified by nested PCR using previously described degenerate primer sets and Accurate Biology reverse transcriptase (cat. no. AG12501) for the first round, followed by Phusion High-Fidelity DNA Polymerase (NEB, cat. no. M0530S) for the second round. PCR products were purified and sequenced by Sanger sequencing (Detaibio, cat. no. DTT06). V(D)J gene segment usage, complementarity-determining region (CDR) sequences, and somatic hypermutation frequencies were analyzed using the IMGT/HighV-QUEST web portal (http://www.imgt.org). Somatic hypermutation frequencies were calculated as 100 minus the percentage identity of the V-REGION

to the closest germline V allele using IMGT/HighV-QUEST; junctional diversity in CDR3 was not included in this metric.

Epitope classification by AlphaFold3 structural modeling and CDR-active-site distance analysis

For each of the 28 clonotypes, the VH and VL amino acid sequences were used to model the variable fragment in complex with *A. stephensi* CPB using AlphaFold3[50] (AlphaFold Server, default parameters; complexes generated in batch), with the CPB component predicted de novo from the *A. stephensi* CPB amino acid sequence. For each complex, the model with the highest ipTM score was selected for analysis. The CPB chain was identified by global sequence alignment, and the eleven active-site pocket residues (Arg^{189}/Arg^{259}/His^{308}/Tyr^{310}/Val^{358}/Leu^{359}/Tyr^{360}/ Gly^{364}/Ala^{365} /Asp^{367}/Phe^{391}) were mapped onto the model coordinate system to correct for any N-terminal offset introduced during construct design. Complementarity-determining regions (CDRs) were annotated according to the IMGT unique numbering, with CDR boundaries localized in each modeled chain using the conserved framework-4 motifs as anchors. The CDR-pocket distance was defined as the minimum distance between any heavy atom of the CDR loops and any heavy atom of the eleven pocket residues, computed separately for the heavy and light chains and reported as the smaller of the two values, following the intermolecular contact definition established for protein-protein complexes [51].

Using the 8 Å residue-contact threshold established in previous structural modeling studies[52], clonotypes with a CDR–pocket distance below 8 Å were classified as active site-targeting (AST), whereas those with a distance equal to or greater than 8 Å were classified as non-active-site-targeting (non-AST). All assignments and structural measurements were performed with PyMOL (version 2.5.4, Schrödinger).

Monoclonal antibody preparation

Selected VH and VL sequences were cloned into a mouse IgG3 expression backbone and transfected into Expi293F cells (Thermo Fisher, cat. no. A14527) using ExpiFectamine 293 Transfection Kit (Thermo Fisher, cat. no. A14525) according to the manufacturer's protocol. Culture supernatants were harvested at day 5 post-transfection, and antibodies were purified by Protein A affinity chromatography (HiTrap MabSelect Sure, Cytiva, cat. no. 11003494), dialyzed against PBS, and concentrated to 1-2 mg/mL. Purity was assessed by SDS-PAGE under reducing conditions.

For epitope binding characterization, 96-well plates were coated with 1 μg/mL wild-type or mutant rCPB in carbonate buffer (pH 9.6) overnight at 4°C. After blocking with 3% (w/v) bovine serum albumin (BSA; Sigma-Aldrich, cat. no. A9418) in PBS-T (PBS + 0.05% Tween-20) for 2 hours at 37°C, purified mAbs were added at serial dilutions (0.01-10 μg/mL) and incubated for 1 hour at 37°C. Bound antibodies were detected with HRP-conjugated goat anti-mouse IgG (Jackson ImmunoResearch, cat. no. 115-035-003) and TMB substrate. Relative binding was normalized to wild-type CPB binding (set to 1.0).

Alanine-scanning epitope mapping

Sixteen residues within the predicted antibody–CPB interfaces (Arg^{32}, Glu^{34}, Arg^{36}, Glu^{37}, Leu^{60}, Gly^{61}, Arg^{62}, Asn^{63}, Asp^{84}, Gly^{311}, Glu^{329}, Arg^{333}, Glu^{349}, Glu^{351}, Asp^{357}, and Thr^{418}) were individually substituted with alanine by overlap extension PCR using Phusion High-Fidelity DNA Polymerase (NEB, cat. no. M0530S). Mutant proteins were expressed and purified as described for wild-type rCPB. The binding of mAbE8, mAbC8, and mAbD8 to each mutant was quantified by ammonium thiocyanate (NH_4SCN) dissociation ELISA: 96-well plates were coated with wild-type or mutant rCPB, incubated with each mAb, and bound antibodies were subjected to stepwise chaotrope elution with NH_4SCN at final concentrations of 0.5, 1, 2, and 3 M prior to detection with HRP-conjugated goat anti-mouse IgG. Relative binding (avidity index) was calculated as (OD_{450} of mutant/OD_{450} of wild-type), with wild-type binding set to 1.0.

Targeted metabolomic analysis

For metabolomic profiling, fully engorged female mosquitoes from each group were dissected at 24 hours PBM. Midguts were rapidly excised in ice-cold PBS, immediately snap-frozen in liquid nitrogen, and stored at -80°C until analysis.

Frozen midgut samples (pooled from 30 mosquitoes per biological replicate, 3 replicates per group) were homogenized in 500 μL of ice-cold methanol: water (4:1, v/v) containing internal standards (L-2-chlorophenylalanine, 0.05 mg/mL) using a TissueLyser II (Qiagen) at 30 Hz for 2 minutes. After centrifugation at 12,000 × g for 10 minutes at 4°C, the supernatant was collected and evaporated to dryness under nitrogen. Dried extracts were reconstituted in 100 μL of 5% acetonitrile in water containing 0.1% formic acid.

Targeted metabolites were quantified by UHPLC–MS/MS on an ACQUITY UPLC I-Class system coupled to a Xevo TQ-S triple-quadrupole mass spectrometer (Waters). Chromatographic

separation was carried out on an ACQUITY BEH C18 column (2.1 × 100 mm, 1.7 µm; Waters, cat. no. 186002352) maintained at 40 °C, with water containing 0.1% formic acid as phase A and acetonitrile containing 0.1% formic acid as phase B, at a flow rate of 0.4 mL/min and an injection volume of 5 µL. The linear gradient was as follows: 2% B (0–1 min), 2–30% B (1–8 min), 30–95% B (8–10 min), 95% B (10–11 min), 95–2% B (11–11.5 min), and 2% B (11.5–13 min). For mass spectrometry, a capillary voltage of 3.0 kV (positive-ion mode) or 2.5 kV (negative-ion mode) was applied, with a source temperature of 150 °C, a desolvation temperature of 500 °C, and cone and desolvation gas flows of 150 and 1,000 L/h, respectively. A total of 127 amino acid and amino acid-related metabolites were monitored. Raw data were processed in MassLynx v4.2/TargetLynx (Waters); peak areas were normalized to the internal standard and converted to concentrations using calibration curves generated from authentic standards. PCA and volcano plots were generated with MetaboAnalyst 5.0 (https://www.metaboanalyst.ca), and between-group differences were assessed by unpaired two-tailed Student's t-test, with an adjusted $P < 0.05$ considered significant.

Amino acid supplementation experiments

In vitro rescue experiments (membrane feeding). For rescue of antibody-induced phenotypes, L-lysine (Sigma-Aldrich, cat. no. L8662) and L-arginine (Sigma-Aldrich, cat. no. A8094) were supplemented individually into defibrinated blood at final concentrations of 2 mM or 20 mM (individually) prior to the addition of CPB-pAb (final 1 mg/mL). Control blood meals contained equivalent volumes of PBS. Blood mixtures were fed to *A. stephensi* mosquitoes via membrane feeder, and mosquitocidal activity (survival and fecundity) was assessed as described above.

In vivo amino-acid supplementation combined with passive antibody transfer. For experiments combining amino-acid supplementation with passive immunization, BALB/c mice were infected with *Pb*-GFP as described above. On day 3 post-infection, mice received CPB-pAb (10 mg/mL) or monoclonal antibodies (mAbE8, mAbC8 or mAbD8, 400 µg/mL) by tail-vein injection in a total volume of 100 µL, in the presence or absence of L-lysine and L-arginine co-administered by tail-vein injection (2 mM each, 100 µL). Control mice received equivalent volumes of PBS. Fifteen minutes after injection, mice were exposed to mosquitoes for blood feeding, and oocyst development was assessed at day 14 post blood meal as described above.

L-lysine and L-arginine were added in combination (2 mM each) to defibrinated blood containing CPB-pAb or naïve mouse IgG (both 1 mg/mL) and fed to mosquitoes via membrane feeder; control blood meals contained equivalent volumes of PBS. Midguts were dissected at day 3 post blood meal. Relative *cpb* expression was quantified by quantitative RT-PCR (5 mosquitoes per replicate, 5 replicates per group, normalized to *rps7*), and CPB protein was examined by immunofluorescence with DAPI counterstain as described below; epithelial fluorescence intensity was quantified in ImageJ and normalized to DAPI. Data were pooled from 2 independent experiments.

Enzyme-Linked Immunosorbent Assay (ELISA)

The 96-well plates were coated with 1 μg/mL of the target antigen in sodium bicarbonate buffer (pH 9.6) at 4 °C overnight. The plates were washed with PBS-0.05% Tween 20 prior to blocking with 0.1% PBS-casein for 2 hours at 37 °C. Serum samples were added to each well at appropriate dilutions and incubated for 1 hour at 37 °C, followed by incubation with HRP-conjugated secondary antibody under the same conditions. Colour development was performed using 3,3',5,5'-Tetramethylbenzidine (Thermo Scientific, cat. no. 34028). The reaction was stopped using 0.5M H2SO4 and the absorbance was measured at 450 nm. For detecting IgG subclasses, goat anti-mouse IgG1, IgG2a, IgG2b and IgG3 antibodies were used at a dilution of 1:1000 followed by HRP conjugated rabbit anti-goat IgG used at dilution of 1: 5000.

Carboxypeptidase B enzymatic activity assay

Carboxypeptidase B activity was determined spectrophotometrically using hippuryl-L-arginine as the substrate, following the classic method of Folk and Gladner with modification [53]. The assay was conducted at 25 °C in 25 mM Tris-HCl (pH 7.65) containing 0.1 M NaCl. A standard curve was generated using serial dilutions of hippuric acid (0-2.5 mM) in the assay buffer, and the absorbance at 254 nm (A_{254}) versus hippuric acid amount (μmol) was fitted to a linear regression for quantification. For inhibition assays, CPB (17.5 μg/mL) was pre-incubated with monoclonal antibodies (mAbE8/mAbC8/mAbD8) at a 1:1 molar ratio for 15 min at 4 °C; PBS and enzyme-free mixtures served as controls. Reactions were performed in 96-well UV-transparent plates in a total volume of 200 μL per well, containing 100 μL of pre-incubated CPB and 100 μL of 4 mM substrate. After adding CPB solution to the plate and equilibrating at 25 °C for 3 min, the reaction was initiated by rapid substrate addition, and A_{254} was recorded continuously for 5 min. The initial

linear slope (ΔA_{254}/min) was determined from the kinetic curves, and the amount of hippuric acid produced per minute was calculated via the standard curve. Specific activity (U/mg) was derived from the linear phase (0-80 s) and defined as the amount of enzyme releases 1 μmol hippuric acid per minute per mg protein. All assays were performed in triplicates independently.

Quantitative RT-PCR

Midguts and other tissues were collected at indicated times post-blood meal (5 mosquitoes pooled per replicate), and total RNA was extracted using TRIzol (Thermo Fisher Scientific, cat. no. 15596026). First-strand cDNA was synthesized from 1 μg RNA using PrimeScript RT Master Mix (Accurate Biology, cat. no. AG11705), and qPCR was performed using SYBR Green Premix Pro Taq HS (Accurate Biology, cat. no. AG11733) on a StepOnePlus system (Applied Biosystems). The ribosomal protein S7 (rps7) gene served as the endogenous reference, and relative expression was calculated by the $2^{\wedge(-\Delta\Delta Ct)}$ method. Primer sequences are listed in Supplementary table 1.

Western blot analysis

Protein samples were denatured in Laemmli buffer containing 50 mM DTT (Sigma-Aldrich, cat. no. D0632), resolved by 12% SDS-PAGE, and transferred to PVDF membranes (Merck, cat. no. ISEQ00010). Membranes were probed with mouse anti-CPB polyclonal antibody (1:5,000) or rabbit anti-HSP70 (1:5,000; Thermo Fisher, cat. no. MA3-006), followed by goat anti-mouse IgG-HRP (1:5,000; Jackson ImmunoResearch, cat. no. 115-035-003) secondary antibody. Bands were visualized with ECL (Merck, cat. no. WBKLS0500) and quantified using Image Lab (Bio-Rad).

Immunohistochemistry and immunofluorescence

Paraffin-embedded tissue sections (5 μm) were processed by standard deparaffinization, citrate-based antigen retrieval, and blocking. For IHC, sections were incubated overnight at 4°C with mouse anti-CPB antibody (1:5,000), followed by biotinylated secondary antibody and streptavidin-HRP (Vectastain ABC Kit, Vector Laboratories), developed with DAB, and imaged on an Olympus BH-2 microscope. For the detection of mouse IgG distribution in mosquito tissues, sections were incubated directly with the anti-mouse secondary antibody (1:200; Jackson ImmunoResearch, cat. no. 115-035-003) without primary antibody, and processed using the same conditions described above. For immunofluorescence, sections were incubated with mouse anti-CPB antibody (1:2,000), followed by Alexa Fluor 488-conjugated goat anti-mouse IgG (1:1,000; Thermo Fisher, cat. no. A-11001), counterstained with DAPI, mounted in ProLong Gold (Thermo

Fisher, cat. no. P36930), and imaged on an Olympus FV3000 confocal microscope. Fluorescence intensity was quantified in ImageJ as mean gray values of midgut epithelium ROIs normalized to DAPI.

Statistical analysis

Comparisons between two groups were performed using the unpaired two-tailed Student's t-test, and comparisons among multiple groups using the Kruskal-Wallis test followed by Dunn's multiple comparisons test. Survival curves were compared using the log-rank (Mantel-Cox) test. The linear relationship between variables was determined by Pearson's correlation coefficient. Categorical data (infection prevalence, oviposition rates) were analyzed by the chi-square test or Fisher's exact test, as appropriate. A two-tailed P value < 0.05 was considered statistically significant. Data are presented as individual data points with medians or as indicated in the figure legends. Exact P values and statistical tests used for each experiment are reported in the corresponding figure legends.

Data availability

All data supporting the findings of this study are available within the paper and its Supplementary Information. Source data are provided with this paper.

REFERENCES

1 World Health Organization. World Malaria Report 2025 https://www.who.int/teams/global-malaria-programme/reports/world-malaria-report-2025 (WHO, Geneva, 2025).

2 Zhang, S. X. *et al.* Global, regional, and national burden of malaria, 1990–2021: Findings from the global burden of disease study 2021. *Decoding Infection and Transmission* **2**, 100030 (2024). https://doi.org/10.1016/j.dcit.2024.100030

3 Vitiello, A. & Zovi, A. The status of malaria, challenges and opportunities to end malaria: an editorial. *European Journal of Clinical Microbiology & Infectious Diseases* **44**, 1761-1762 (2025). https://doi.org:10.1007/s10096-025-05160-2

4 Dennis, T. P. W. *et al.* The origin, history, and resistance architecture of an invasive urban malaria mosquito in Africa. *Science (New York, N.Y.)* **393**, eadx6925 (2026). https://doi.org:doi:10.1126/science.adx6925

5 Balaska, S. *et al.* Predictive chemoproteomics and functional validation reveal Coeae6g-mediated insecticide cross-resistance in the malaria vector Anopheles gambiae. *Nature communications* **16**, 10772 (2025). https://doi.org:10.1038/s41467-025-65827-4

6 He, M., Chen, Y., Yang, H. & Li, Y. Mosquitoes as pesticide disseminators: Advancing pyriproxyfen-based technologies for next-generation vector control. *Decoding Infection and Transmission* **3**, 100059 (2025). https://doi.org/10.1016/j.dcit.2025.100059

7 Healy, S. *et al.* A Vaccine to Block Plasmodium falciparum Transmission. *NEJM Evidence* **4** (2025). https://doi.org:10.1056/EVIDoa2400188

8 Alkema, M. *et al.* A Pfs48/45-based vaccine to block Plasmodium falciparum transmission: phase 1, open-label, clinical trial. *BMC medicine* **22**, 170 (2024). https://doi.org:10.1186/s12916-024-03379-y

9 Sagara, I. *et al.* Malaria transmission-blocking vaccines Pfs230D1-EPA and Pfs25-EPA in Alhydrogel in healthy Malian adults; a phase 1, randomised, controlled trial. *The Lancet Infectious Diseases* **23**, 1266-1279 (2023). https://doi.org/10.1016/S1473-3099(23)00276-1

10 Sagara, I. *et al.* Safety and immunogenicity of Pfs25H-EPA/Alhydrogel, a transmission-blocking vaccine against Plasmodium falciparum: a randomised, double-blind, comparator-controlled, dose-escalation study in healthy Malian adults. *The Lancet Infectious Diseases* **18**, 969-982 (2018). https://doi.org/10.1016/S1473-3099(18)30344-X

11 Tiono, A. *et al.* A randomized first-in-human phase I trial of differentially adjuvanted Pfs48/45 malaria vaccines in Burkinabé adults. *Journal of Clinical Investigation* **134**, e175707 (2024). https://doi.org:10.1172/JCI175707

12 Dinglasan, R. R. *et al.* Disruption of Plasmodium falciparum development by antibodies against a conserved mosquito midgut antigen. *Proceedings of the National Academy of Sciences of the United States of America* **104**, 13461-13466 (2007). https://doi.org:10.1073/pnas.0702239104

13 Dinglasan, R. R. & Jacobs-Lorena, M. Flipping the paradigm on malaria transmission-blocking vaccines. *Trends in parasitology* **24**, 364-370 (2008). https://doi.org:10.1016/j.pt.2008.05.002

14 Lavazec, C. & Bourgouin, C. Mosquito-based transmission blocking vaccines for interrupting Plasmodium development. *Microbes and Infection* **10**, 845-849 (2008). https://doi.org/10.1016/j.micinf.2008.05.004

15 Smith, D. L. & McKenzie, F. E. Statics and dynamics of malaria infection in Anopheles mosquitoes. *Malaria journal* **3**, 13 (2004). https://doi.org:10.1186/1475-2875-3-13

16 Dolan, B. *et al.* mosGILT antibodies interfere with Plasmodium sporogony in Anopheles gambiae. *Nature communications* **16**, 592 (2025). https://doi.org:10.1038/s41467-025-55902-1

17 Niu, G. *et al.* The fibrinogen-like domain of FREP1 protein is a broad-spectrum malaria transmission-blocking vaccine antigen. *J Biol Chem* **292**, 11960-11969 (2017). https://doi.org:10.1074/jbc.M116.773564

18 Lavazec, C. *et al.* Carboxypeptidases B of Anopheles gambiae as targets for a Plasmodium falciparum transmission-blocking vaccine. *Infection and immunity* **75**, 1635-1642 (2007). https://doi.org:10.1128/iai.00864-06

19 Moskalyk, L. A. Carboxypeptidase B in Anopheles gambiae (Diptera: Culicidae): effects of abdominal distention and blood ingestion. *Journal of medical entomology* **35**, 216-221 (1998). https://doi.org:10.1093/jmedent/35.3.216

20 Lavazec, C., Bonnet, S., Thiery, I., Boisson, B. & Bourgouin, C. cpbAg1 encodes an active carboxypeptidase B expressed in the midgut of Anopheles gambiae. *Insect molecular biology* **14**, 163-174 (2005). https://doi.org:10.1111/j.1365-2583.2004.00541.x

21 Zisapel, N., Kurn-Abramowitz, N. & Sokolovsky, M. Basic and non-basic substrates of carboxypeptidase B. *Eur J Biochem* **35**, 507-511 (1973). https://doi.org:10.1111/j.1432-1033.1973.tb02866.x

22 Gavor, E. *et al.* Structure of Aedes aegypti procarboxypeptidase B1 and its binding with Dengue virus for controlling infection. *Life Sci Alliance* **5** (2022). https://doi.org:10.26508/lsa.202101211

23 Lampe, L., Jentzsch, M., Kierszniowska, S. & Levashina, E. A. Metabolic balancing by miR-276 shapes the mosquito reproductive cycle and Plasmodium falciparum development. *Nature communications* **10**, 5634 (2019). https://doi.org:10.1038/s41467-019-13627-y

24 Raz, A., Dinparast Djadid, N. & Zakeri, S. Molecular characterization of the carboxypeptidase B1 of Anopheles stephensi and its evaluation as a target for transmission-blocking vaccines. *Infection and immunity* **81**, 2206-2216 (2013). https://doi.org:10.1128/iai.01331-12

25 Mongkol, W., Arunyawat, U., Surat, W. & Kubera, A. Active Compounds Against Anopheles minimus Carboxypeptidase B for Malaria Transmission-Blocking Strategy. *Journal of medical entomology* **52**, 1322-1332 (2015). https://doi.org:10.1093/jme/tjv133

26 Pomun, T., Wonginta, P. & Kubera, A. Malaria Box Compounds against Anopheles gambiae (Diptera: Culicidae) Carboxypeptidase B Activity to Block Malaria Transmission. *Journal of medical entomology* **59**, 1355-1362 (2022). https://doi.org:10.1093/jme/tjac043

27 Rismani, E., Mafakher, L., Asgari, M. & Raz, A. Leech, potato, and tomato carboxypeptidase inhibitors against Anopheles stephensi carboxypeptidase B1 and B2. *Archives of Biochemistry and Biophysics* **759**, 110086 (2024). https://doi.org/10.1016/j.abb.2024.110086

28 Geng, G. *et al.* Viral and non-viral vectors in gene therapy: current state and clinical perspectives. *eBioMedicine* **118**, 105834 (2025). https://doi.org/10.1016/j.ebiom.2025.105834

29 Greig, J. A. *et al.* Integrated vector genomes may contribute to long-term expression in primate liver after AAV administration. *Nature Biotechnology* **42**, 1232-1242 (2024). https://doi.org:10.1038/s41587-023-01974-7

30 Zabaleta, N. *et al.* An AAV-based, room-temperature-stable, single-dose COVID-19 vaccine provides durable immunogenicity and protection in non-human primates. *Cell host & microbe* **29**, 1437-1453.e1438 (2021). https://doi.org/10.1016/j.chom.2021.08.002

31 Wu, F. *et al.* Single-shot AAV-vectored vaccine against SARS-CoV-2 with fast and long-lasting immunity. *Acta Pharmaceutica Sinica B* **13**, 2219-2233 (2023). https://doi.org/10.1016/j.apsb.2022.07.004

32 Shahnaij, M. *et al.* Liver-Directed AAV8 Booster Vaccine Expressing Plasmodium falciparum Antigen Following Adenovirus Vaccine Priming Elicits Sterile Protection in a Murine Model. *Frontiers in immunology* **12**, 612910 (2021). https://doi.org:10.3389/fimmu.2021.612910

33 Yusuf, Y. *et al.* Adeno-Associated Virus as an Effective Malaria Booster Vaccine Following Adenovirus Priming. *Frontiers in immunology* **10**, 730 (2019). https://doi.org:10.3389/fimmu.2019.00730

34 Saul, A. Zooprophylaxis or zoopotentiation: the outcome of introducing animals on vector transmission is highly dependent on the mosquito mortality while searching. *Malaria journal* **2**, 32 (2003). https://doi.org:10.1186/1475-2875-2-32

35 Zhou, L. *et al.* Long-term protection against human papillomavirus e7-positive tumor by a single vaccination of adeno-associated virus vectors encoding a fusion protein of inactivated e7 of human papillomavirus 16/18 and heat shock protein 70. *Human gene therapy* **21**, 109-119 (2010). https://doi.org:10.1089/hum.2009.139

36 Steel, J. C. *et al.* Oral vaccination with adeno-associated virus vectors expressing the Neu oncogene inhibits the growth of murine breast cancer. *Molecular therapy : the journal of the American Society of Gene Therapy* **21**, 680-687 (2013). https://doi.org:10.1038/mt.2012.260

37 Avilés, F. X. & Vendrell, J. in *Handbook of Proteolytic Enzymes (Third Edition)* (eds Neil D. Rawlings & Guy Salvesen) 1324-1329 (Academic Press, 2013).

38 Pourhashem, Z. *et al.* Malaria transmission blocking activity of Anopheles stephensi alanyl aminopeptidase N antigen formulated with MPL, CpG, and QS21 adjuvants. *PloS one* **19**, e0306664 (2024). https://doi.org:10.1371/journal.pone.0306664

39 Scally, S. W. *et al.* Molecular definition of multiple sites of antibody inhibition of malaria transmission-blocking vaccine antigen Pfs25. *Nature communications* **8**, 1568 (2017). https://doi.org:10.1038/s41467-017-01924-3

40 Kundu, P. *et al.* Structural delineation of potent transmission-blocking epitope I on malaria antigen Pfs48/45. *Nature communications* **9**, 4458 (2018). https://doi.org:10.1038/s41467-018-06742-9

41 Srivastava, A. *et al.* Stage-Specific Changes in Plasmodium Metabolism Required for Differentiation and Adaptation to Different Host and Vector Environments. *PLoS pathogens* **12** (2017). https://doi.org:10.1371/journal.ppat.1006094

42 Rodrigues, J., Brayner, F. A., Alves, L. C., Dixit, R. & Barillas-Mury, C. Hemocyte Differentiation Mediates Innate Immune Memory in Anopheles gambiae Mosquitoes. *Science (New York, N.Y.)* **329**, 1353-1355 (2010). https://doi.org:10.1126/science.1190689

43 Barletta, A. B. F., Trisnadi, N., Ramirez, J. L. & Barillas-Mury, C. Mosquito Midgut Prostaglandin Release Establishes Systemic Immune Priming. *iScience* **19**, 54-62 (2019). https://doi.org/10.1016/j.isci.2019.07.012

44 Ramirez, J. L. *et al.* A mosquito lipoxin/lipocalin complex mediates innate immune priming in Anopheles gambiae. *Nature communications* **6**, 7403 (2015). https://doi.org:10.1038/ncomms8403

45 Noriega, F. G. & Wells, M. A. A molecular view of trypsin synthesis in the midgut of Aedes aegypti. *Journal of Insect Physiology* **45**, 613-620 (1999). https://doi.org/10.1016/S0022-1910(99)00052-9

46 Donnelly, B., Berrang-Ford, L., Ross, N. A. & Michel, P. A systematic, realist review of zooprophylaxis for malaria control. *Malaria journal* **14**, 313 (2015). https://doi.org:10.1186/s12936-015-0822-0

47 Kanatani, S., Stiffler, D., Bousema, T., Yenokyan, G. & Sinnis, P. Revisiting the Plasmodium sporozoite inoculum and elucidating the efficiency with which malaria parasites progress through the mosquito. *Nature communications* **15**, 748 (2024). https://doi.org:10.1038/s41467-024-44962-4

48 Espinosa, D. A. *et al.* Robust antibody and CD8(+) T-cell responses induced by P. falciparum CSP adsorbed to cationic liposomal adjuvant CAF09 confer sterilizing immunity against experimental rodent malaria infection. *NPJ vaccines* **2** (2017). https://doi.org:10.1038/s41541-017-0011-y
49 Liu, C. *et al.* Mosaic RBD nanoparticle elicits immunodominant antibody responses across sarbecoviruses. *Cell Reports* **43** (2024). https://doi.org:10.1016/j.celrep.2024.114235
50 Abramson, J. *et al.* Accurate structure prediction of biomolecular interactions with AlphaFold 3. *Nature* **630**, 493-500 (2024). https://doi.org:10.1038/s41586-024-07487-w
51 Vangone, A. & Bonvin, A. M. Contacts-based prediction of binding affinity in protein-protein complexes. *eLife* **4**, e07454 (2015). https://doi.org:10.7554/eLife.07454
52 Ovchinnikov, S. *et al.* Protein structure determination using metagenome sequence data. *Science (New York, N.Y.)* **355**, 294-298 (2017). https://doi.org:10.1126/science.aah4043
53 Folk, J. E. & Gladner, J. A. CARBOXYPEPTIDASE B: I. PURIFICATION OF THE ZYMOGEN AND SPECIFICITY OF THE ENZYME. *Journal of Biological Chemistry* **231**, 379-391 (1958). https://doi.org:https://doi.org/10.1016/S0021-9258(19)77314-1

Acknowledgments: We thank Prof Bo Shen from Nanjing Medical University and staff of the Jiangsu Institute of Parasitic Diseases for assisting the initial establishment of insectary. The Pb-GFP line was a gift from Prof Ian Cockburn of The Australian National University. This work was also supported by the Analysis and Testing Center of Nanjing Medical University.

Funding: This work was supported by the National Key R&D Program of China (No. 2023YFA1801004), the Prevention and Control of Emerging and Major Infectious Diseases-National Science and Technology Major Project (Grant No. 2026ZD01910803), and the National Natural Science Foundation of China (Grant No. 82472312).

Author Contributions:

Conceptualization: J.Z., J.L., and G.F.; methodology: J.Z., J.L., X.Y., Z.R., J.T., S.B.G., J.C., J.A.C., and G.F.; investigation: J.L., J.Z., X.Y., Z.R., Q.Z., Y.Y., W.H., Y.L., and S.B.G.; visualization: J.Z., J.L., and G.F.; funding acquisition: J.C. and G.F.; supervision: G.F., J.C., W.D., J.B., and J.A.C.; writing—original draft: J.Z., J.L., G.F., J.C., Y.Y., Y.L.Y., S.B.G., J.B., Z.R., J.A.C., J.T., Q.Z., W.D., W.H., X.Y., and Y.L.; writing—review and editing: J.Z., J.L., G.F., J.C., Y.Y., Y.L.Y., S.B.G., J.B., Z.R., J.A.C., J.T., Q.Z., W.D., W.H., X.Y., and Y.L. All authors read and approved the final version of the manuscript.

Competing Interests

All authors declare that they have no competing interests.

Declarations

Clinical trial number: not applicable.

Figures

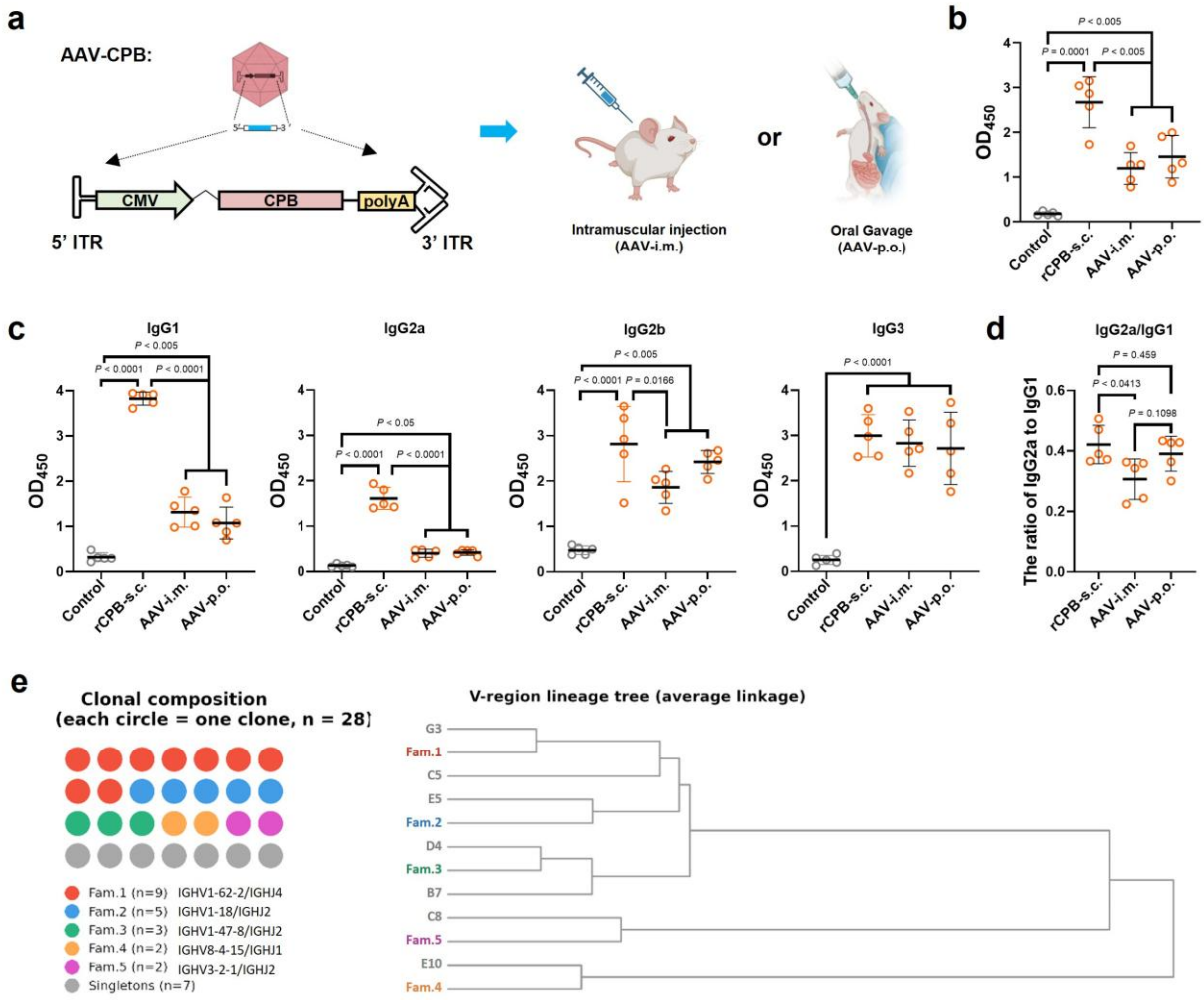
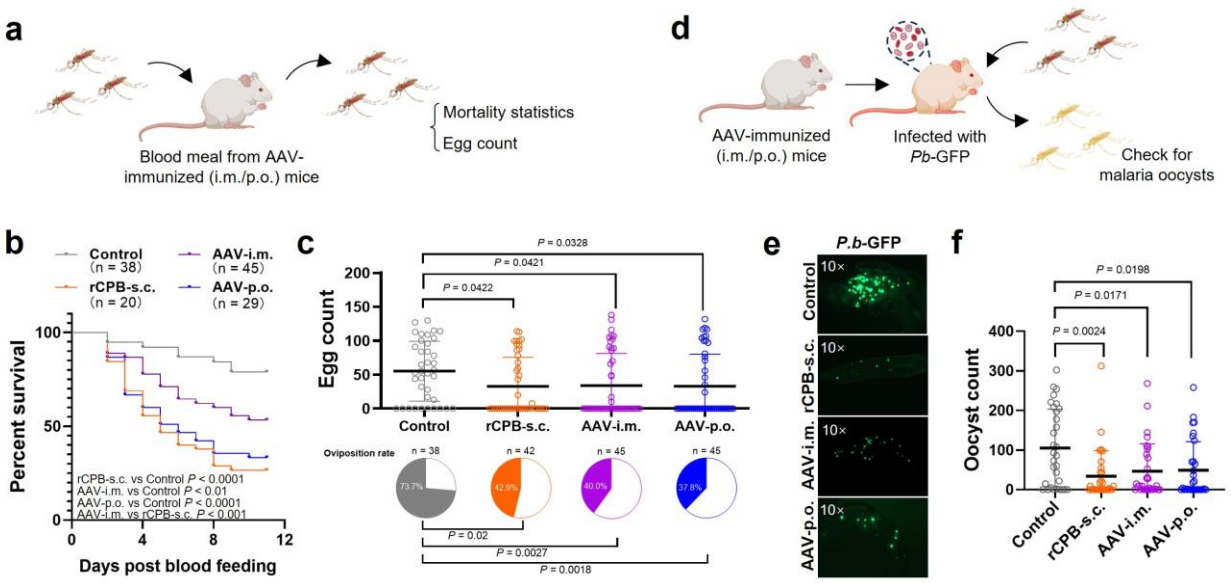


Figure 1. Induction of antibody responses upon AAV-CPB immunization

a Schematic of the AAV-CPB vector construct (left) and immunization scheme (right). The AAV vector contains a CMV promoter-driven CPB expression cassette flanked by 5′ and 3′ inverted terminal repeats (ITRs). Mice were immunized via intramuscular injection (AAV-i.m.) or oral gavage (AAV-p.o.). Recombinant CPB formulated with Freund's adjuvant and administered subcutaneously (rCPB-s.c.) was used as the positive control. **b** CPB-specific IgG antibodies were robustly induced by day 42 post-immunization in both AAV groups. **c** The AAV vaccine elicited IgG subclass profiles dominated by IgG2b and IgG3, which differed significantly from the profile induced by rCPB-s.c (Kruskal-Wallis test followed by Dunn's multiple comparisons test). **d** The IgG2a/IgG1 ratio was significantly lower in the AAV-i.m. group than in the rCPB control group. Data are presented as mean ± SD with individual data points shown; n = 5 mice per group. **e** Clonal architecture of the 28 retrieved clonotypes, showing five expanded families (Fam.1-5, n = 21 sequences) and seven singletons (grey). Each circle represents one clone, with colours denoting clonal families and gray denoting singletons. Five expanded families were identified, including Fam.1 (n = 9, IGHV1-62-2/IGHJ4), Fam.2 (n = 5, IGHV1-

18/IGHJ2), Fam.3 (n = 3, IGHV1-47-8/IGHJ2), Fam.4 (n = 2, IGHV8-4-15/IGHJ1), and Fam.5 (n = 2, IGHV3-2-1/IGHJ2); singletons (n = 7) are shown in gray. Right: V-region lineage tree (average linkage) of the 28 clonotypes illustrating the clonal relationships and lineage diversification among CPB-specific antibodies. Singleton clonotypes are labelled by clone ID (G3, C5, E5, D4, B7, C8 and E10); clonal families are colour-coded as in the left panel.



933

934 **Figure 2. AAV-CPB Vaccine immunization induced both mosquitocidal and transmission-blocking**
935 **efficacy.**

936 **a** Schematic of the direct feeding assay: *A. stephensi* mosquitoes were fed on AAV-CPB-immunized (i.m. or
937 p.o.) or control mice, and mosquito mortality and egg counts were monitored; rCPB-s.c. served as the positive
938 control vaccine. **b** Mosquitoes fed on AAV-CPB-immunized mice exhibited drastically shortened survival (mean
939 survival 8.20 days i.m., 6.69 days p.o., versus 9.89 days control; all $P < 0.01$). Percent survival was monitored
940 for 11 days; P values by log-rank (Mantel–Cox) test. **c** Oviposition was markedly reduced: oviposition rates
941 decreased from 73.7% in the control group to 40.0% (i.m., $P = 0.0027$) and 37.8% (p.o., $P = 0.0018$). Egg counts
942 were analysed by Kruskal-Wallis test with Dunn's multiple-comparisons test; oviposition rates were analysed by
943 chi-square test or Fisher's exact test. **d** Schematic of the transmission-blocking assay: mosquitoes were fed on
944 AAV-CPB-immunized mice infected with *Pb*-GFP, and oocyst development was assessed. **e** Representative
945 fluorescence microscopy images (10×) of *Pb*-GFP oocysts in mosquito midguts. **f** Oocyst loads were
946 significantly reduced in both the i.m. ($P = 0.0171$) and p.o. ($P = 0.0198$) groups compared with controls. Data
947 were analyzed by Kruskal-Wallis test with Dunn's multiple-comparisons test; n = 31 mosquitoes per group. Data
948 are presented as mean ± SD with individual data points shown.

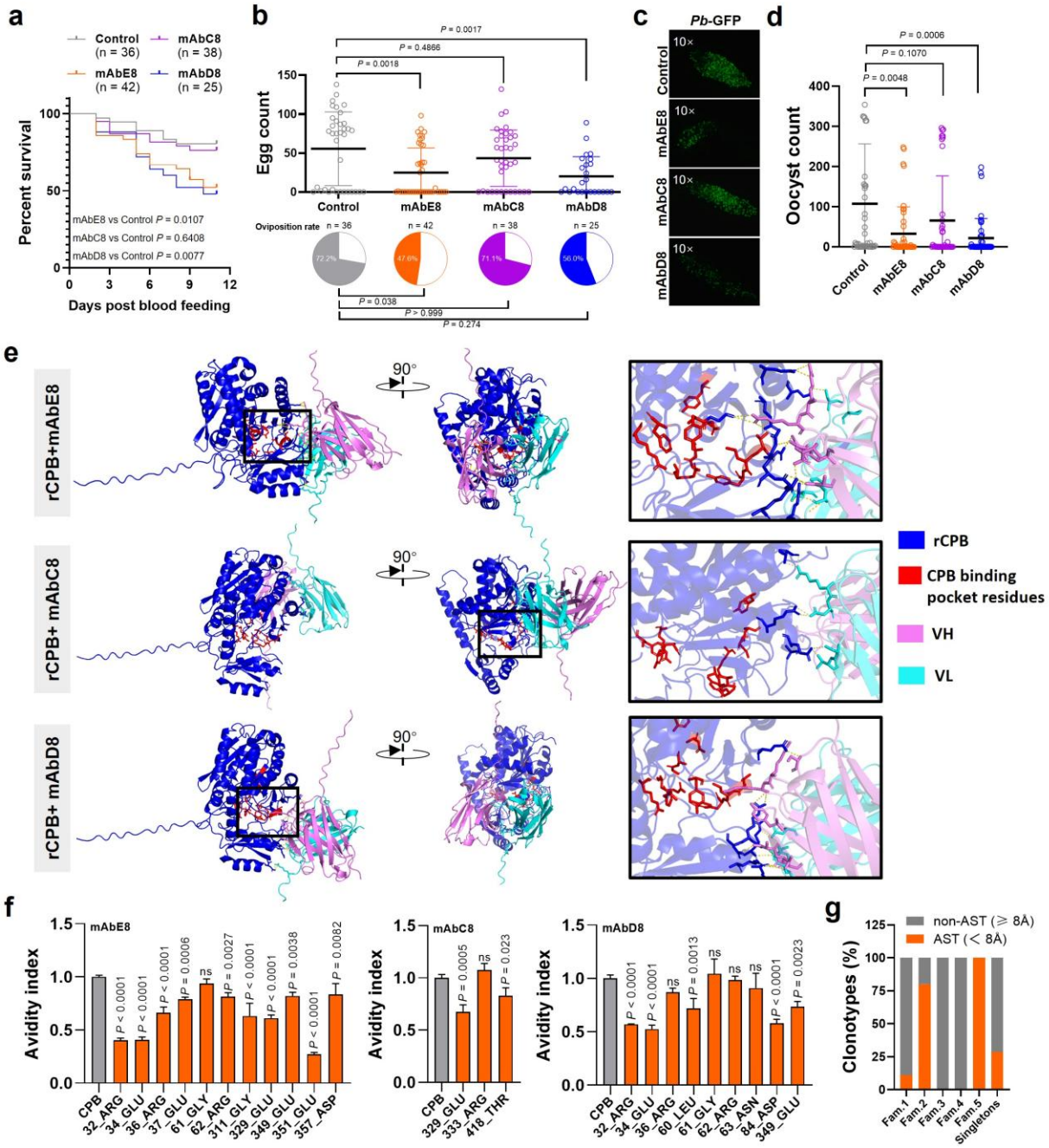


Figure 3. Characterization of the AAV-CPB vaccine-induced functional monoclonal antibodies.

a mAbE8 and mAbD8, but not mAbC8, exhibited potent mosquitocidal activity. Percent survival was monitored for 11 days; P values by log-rank (Mantel–Cox) test. **b** Oviposition rates decreased from 72.2% (control) to 47.6% (mAbE8, $P = 0.038$) and 56.0% (mAbD8, $P = 0.274$). Egg counts were analysed by Kruskal-Wallis test with Dunn's multiple-comparisons test; oviposition rates were analysed by chi-square test or Fisher's exact test; n ⩾ 25 mosquitoes per group. **c** Representative fluorescence microscopy images (10×) of *Pb*-GFP oocysts at 14 days

post infection after passive transfer of the indicated mAbs to infected mice. **d** mAbE8 and mAbD8 significantly reduced oocyst counts, whereas mAbC8 had no effect, underscoring the epitope specificity of protection. Data are presented as mean ± SD with individual data points shown; Data were analyzed by Kruskal-Wallis test with Dunn's multiple-comparisons test. **e** AlphaFold3-predicted structures of the mAbs variable fragments in complex with CPB (two orientations, 90° rotation). mAbE8 and mAbD8 are positioned at the rim and entrance of the catalytic pocket and are predicted to restrict substrate access, whereas mAbC8 binds a distal surface remote from the pocket. **f** Alanine-scanning mutagenesis of predicted antibody-CPB contact residues. Avidity of mAbE8 was significantly reduced by substitutions at Arg^{32}, Glu^{34}, Arg^{36}, Glu^{37}, Arg^{62}, Gly^{311}, Glu^{329}, Glu^{349}, Glu^{351} and Asp^{357}, with Glu^{351} Ala causing the strongest disruption. For mAbD8, avidity was reduced by Arg^{32}, Glu^{34}, Leu^{60}, Asp^{84} and Glu^{349}, whereas Arg^{36}, Gly^{61}, Arg^{62} and Asn^{63} had no detectable effect. mAbC8 avidity was reduced only by Glu^{329}Ala and Thr^{418} Ala, with Arg^{333}Ala having no effect. Avidity indexes were determined by ammonium thiocyanate (NH_4SCN) dissociation ELISA and normalized to wild-type CPB binding (set to 1.0); orange bars, alanine-substituted mutants; *P* values versus wild-type CPB are shown above each bar. n = 3 independent experiments. Bars and error bars represent means and SD, respectively. **g** Classification of the 28 clonotypes by AlphaFold3-predicted paratope location: 9 active site-targeting (AST) and 19 non-AST clonotypes, with AST clones enriched in Fam.2 and Fam.5 (Supplementary Fig. 6B, C). ns, not significant.

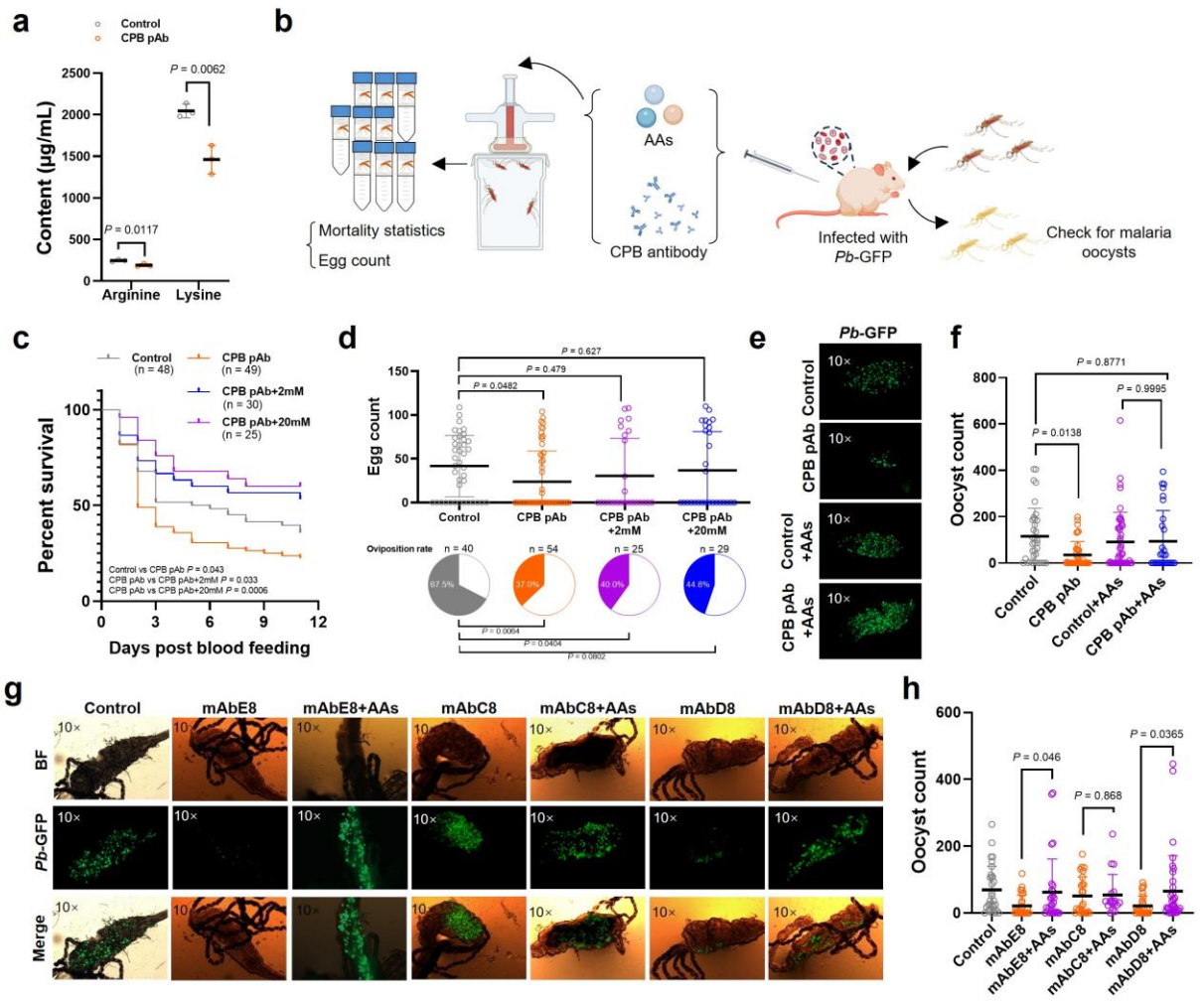


Figure 4. CPB-targeting antibodies restricted amino-acid availability to impair mosquito fitness and *Plasmodium* development.

a Targeted metabolomic analysis showed that CPB-pAb treatment profoundly perturbed amino-acid metabolism (PERMANOVA, $P = 0.001$), specifically reducing the CPB substrates lysine ($P = 0.0062$) and arginine ($P = 0.0117$) in mosquito midguts at 24 h post blood meal. Data are presented as mean ± SD; Statistical significance was determined by two-tailed Student's t-test; 30 of 127 targeted metabolites were differentially abundant (18 up, 12 down). **b** Schematic of the membrane feeding assay with amino acid (AAs) supplementation. Mosquitoes were fed on blood containing CPB antibody with or without exogenous amino acids (2 mM or 20 mM), followed by infection with *Pb*-GFP and assessment of oocyst development. **c** Lysine and arginine supplementation significantly reversed the mosquitocidal activity of CPB-pAb. Percent survival over 11 days; log-rank (Mantel–Cox) test. **d** AAs supplementation rescued egg production and oviposition rates (Egg counts were analyzed by Kruskal-Wallis test with Dunn's multiple-comparisons test; oviposition rates were analyzed by chi-square test or Fisher's exact test). **e** Representative fluorescence microscopy images (10×) of *Pb*-GFP oocysts at 14 days post infection. **f** AAs supplementation attenuated the transmission-blocking effect of CPB-pAb. Data are

presented as mean ± SD with individual data points shown; Data were analyzed by Kruskal-Wallis test with Dunn's multiple-comparisons test. **g** Representative midgut images from mosquitoes fed on *Pb*-GFP-infected mice passively transferred with mAbE8, mAbC8 or mAbD8, with or without AA supplementation. **h** AAs supplementation fully restored *P. berghei* infectivity suppressed by mAbE8 and mAbD8, whereas the non-neutralizing mAbC8 was unaffected. Data are presented as mean ± SD with individual data points shown; Data were analyzed by Kruskal-Wallis test with Dunn's multiple-comparisons test; n ⩾ 20 mosquitoes per group.

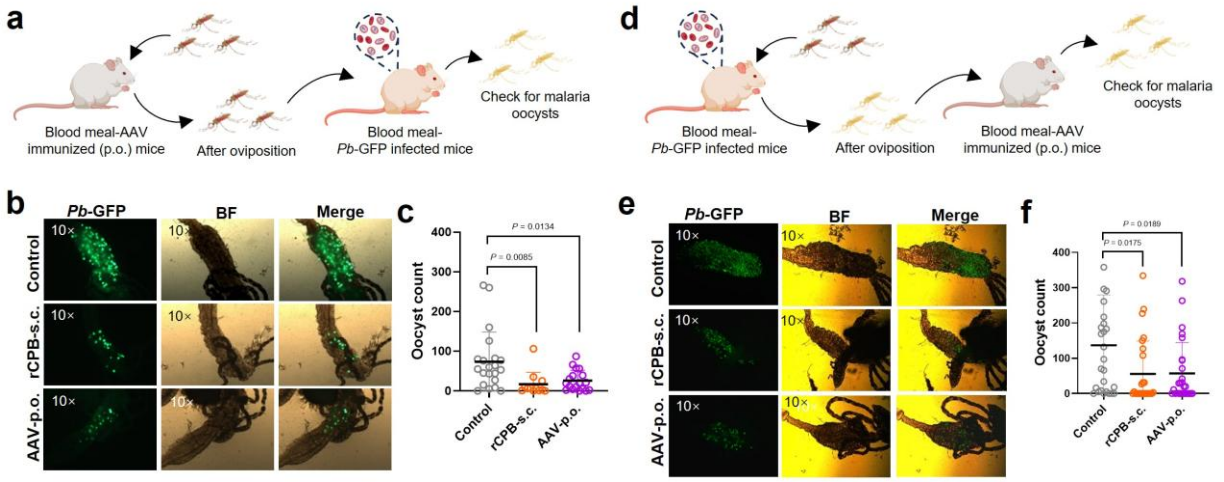


Figure 5. AAV-CPB immunization confers sustained transmission-blocking activity under asynchronous blood-feeding conditions.

a Schematic of the antibody-first asynchronous assay: mosquitoes were fed on blood from mice immunized with AAV-p.o. as the experimental group, rCPB-s.c. as a positive control, or PBS as a negative control; after complete blood meal digestion and oviposition, they were challenged with *Pb*-GFP 3 days after the initial feeding. **b** Representative fluorescence microscopy images (10×) of *Pb*-GFP oocysts at 14 days post infection. BF, bright field. **c** Oocyst counts were significantly reduced in both the rCPB-s.c. and AAV-p.o. groups compared with controls. Data are presented as mean ± SD with individual data points shown; Data were analyzed by Kruskal-Wallis test with Dunn's multiple-comparisons test; n ⩾ 20 mosquitoes per group. **d** Schematic of the reciprocal (parasite-first) assay: mosquitoes were first infected with *Pb*-GFP and allowed to oviposit, then fed on blood from from mice immunized with AAV-p.o. as the experimental group, rCPB-s.c. as a positive control, or PBS as a negative control. **e** Representative fluorescence microscopy images (10×) of oocysts at 14 days post infection. **f** Oocyst counts remained significantly reduced even when antibody exposure occurred after the initial infection. Data are presented as mean ± SD with individual data points shown; Data were analyzed by Kruskal-Wallis test with Dunn's multiple-comparisons test.

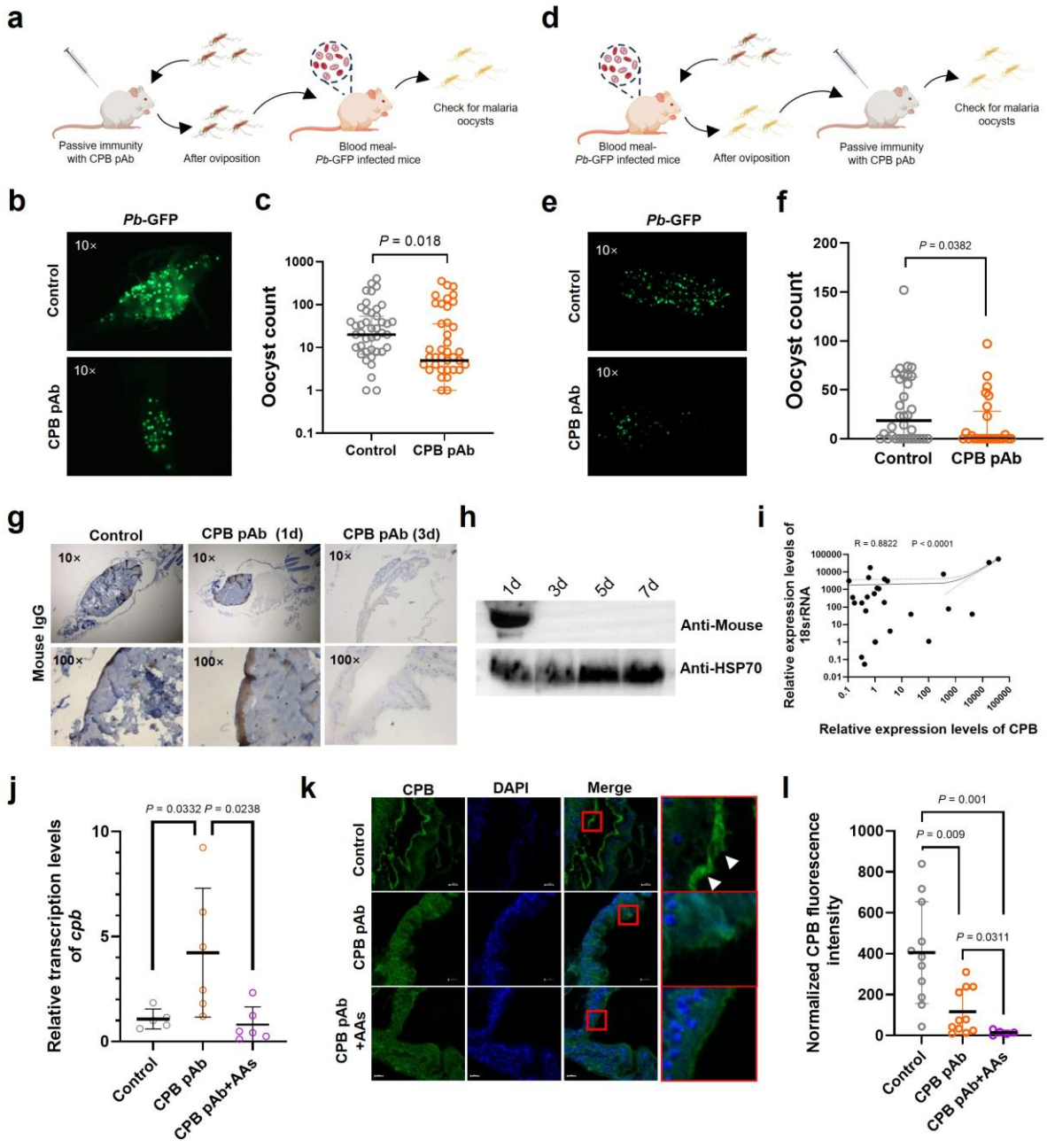
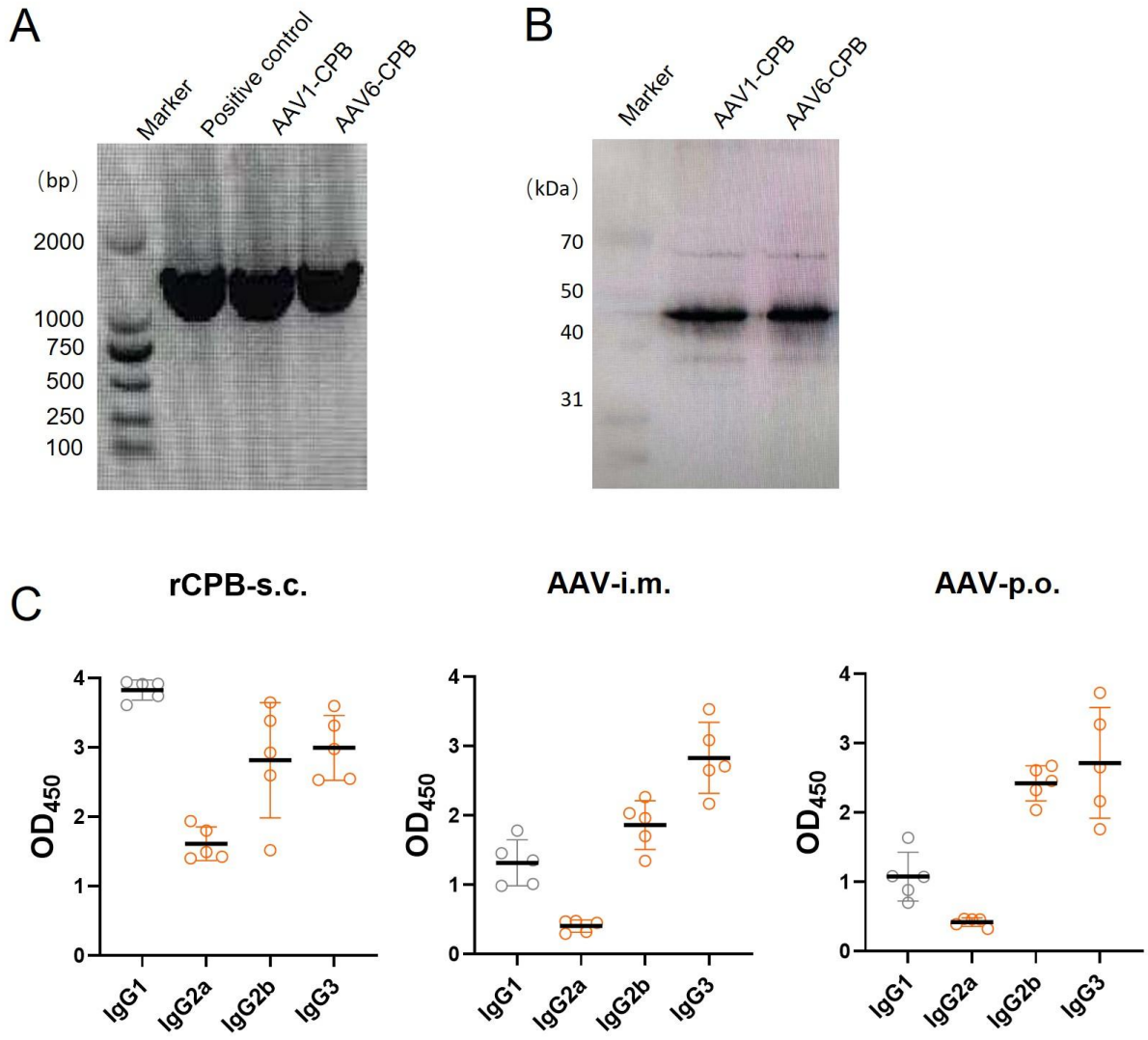


Figure 6. Transient CPB-specific antibody exposure induced sustained transmission-blocking activity accompanied by persistent depletion of endogenous midgut CPB protein.

a Schematic of the antibody-first asynchronous assay: mosquitoes were fed on mice passively immunized with CPB-pAb, and, after complete blood meal digestion and oviposition, challenged with a blood meal from *Pb*-GFP infected mice; oocyst development was examined 14 days later. **b, c** Mosquitoes exposed to CPB-pAb before parasite challenge carried significantly fewer oocysts than controls (P = 0.018). **b** Representative fluorescence microscopy images (10×) of *Pb*-GFP oocysts in mosquito midguts. **c** Oocyst counts per midgut; Data are presented as median ± SD with individual data points shown.; y-axis is log-scaled. **d** Schematic of the

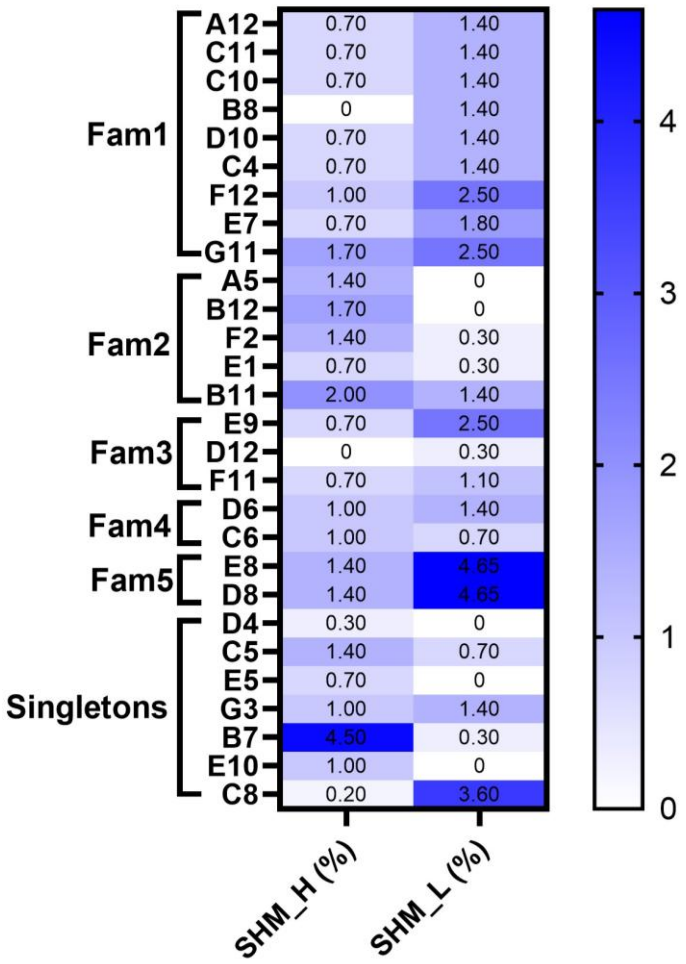
reciprocal (parasite-first) assay: mosquitoes first fed on *Pb*-GFP-infected mice received, after oviposition, a blood meal from passively immunized mice. **e, f** Oocyst counts remained significantly reduced even when CPB-pAb exposure occurred after the infective blood meal ($P = 0.0382$). **e** Representative fluorescence microscopy images (10×). **f** Oocyst counts per midgut; Data are presented as median ± SD with individual data points shown. **b-f**, Statistical significance was determined by two-tailed Student's t-test; n ⩾ 25 mosquitoes per group. **g** Mouse IgG was no longer detectable in mosquito midguts by 3 days post blood meal, as shown by immunohistochemistry of midgut sections from control and CPB-pAb fed mosquitoes at 1 and 3 days post blood meal (10× and 100×). **h** Western blot analysis of mouse IgG in mosquito midgut lysates at the indicated days post blood meal; HSP70 served as the loading control. **i** The *cpb* transcription correlated positively with *Pb*-GFP parasite load (18S rRNA) in mosquito midguts (Pearson R = 0.8822, $P < 0.0001$); both axes are log-scaled. **j** At day 3 post blood meal, CPB-pAb exposure significantly induced *cpb* transcription relative to control ($P = 0.0332$), and this induction was abolished by supplementation with lysine and arginine ($P = 0.0238$, CPB-pAb versus CPB-pAb+AAs). Relative *cpb* expression determined by quantitative RT-PCR and normalized to rps7; Data are presented as mean ± SD with individual data points shown; Kruskal-Wallis test with Dunn's multiple-comparisons test; n = 5 mosquitoes per replicate, 5 replicates per group. **k** Immunofluorescence staining of CPB (green) and DAPI (blue) in mosquito midgut epithelium at day 3 post blood meal; boxed regions are magnified in the rightmost column, and arrowheads indicate CPB localization. n = 11, 11 and 5 epithelial ROIs quantified from 3 midguts per group (2 independent experiments). **l** Quantification of CPB fluorescence intensity normalized to DAPI: both antibody-treated groups were significantly reduced compared with control ($P = 0.009$ and $P = 0.001$, respectively), and the CPB-pAb+AAs group was significantly lower than the CPB-pAb group alone ($P = 0.0311$). Data are presented as mean ± SD with individual data points shown; Kruskal-Wallis test with Dunn's multiple-comparisons test.

Supplementary Information



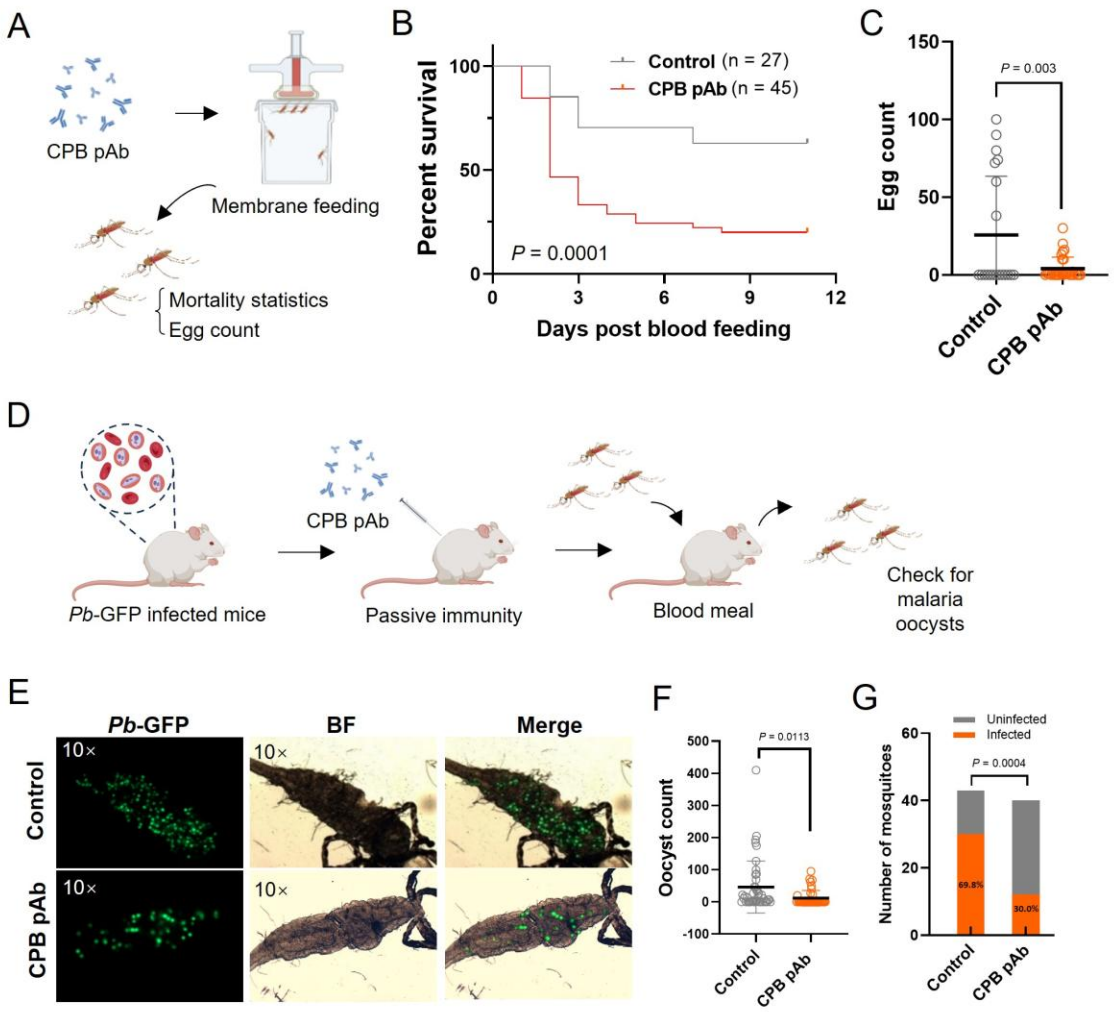
Supplementary Fig. 1. Validation of AAV vector vaccine construct and humoral immune response profiling upon immunization.

(A) Agarose gel electrophoresis confirmed the genomic integrity of the recombinant AAV vectors. **(B)** Western blot analysis confirmed CPB protein expression in producer cells transduced with the AAV vectors. **(C)** The AAV vaccine elicited an IgG subclass profile dominated by IgG2b and IgG3 that differed from the rCPB-s.c. Freund's adjuvant control, with lower IgG2b levels in the AAV-p.o. group. Serum IgG subclasses (IgG1, IgG2a, IgG2b and IgG3) were quantified by ELISA at day 42 post-immunization; Data are presented as mean ± SD with individual data points shown; n = 5 mice per group; Kruskal-Wallis test with Dunn's multiple-comparisons test.



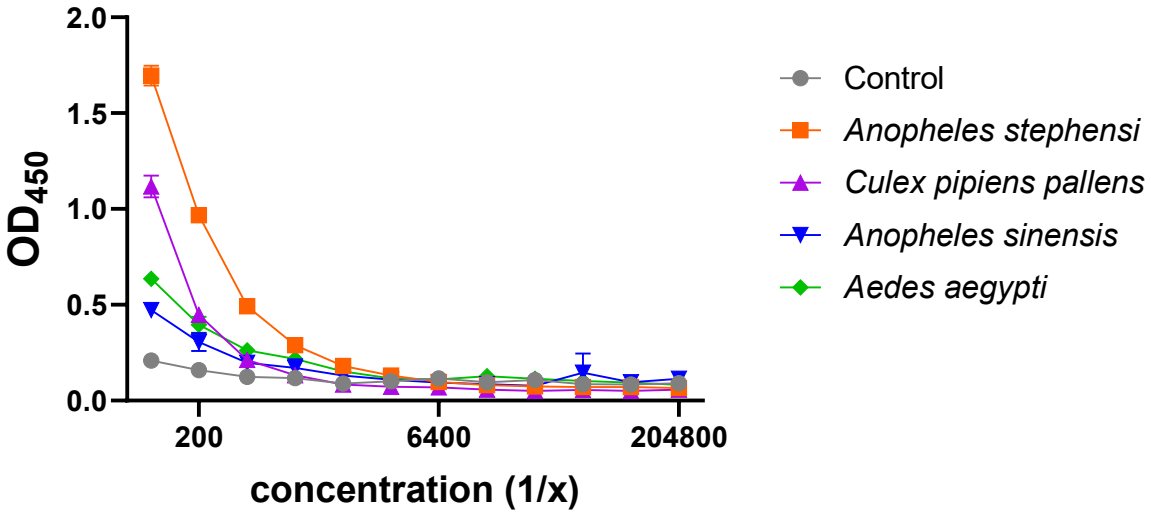
Supplementary Fig. 2. Somatic hypermutation across the V regions of CPB-specific antibody clonotypes.

Heatmap of somatic hypermutation (SHM) frequencies in the heavy-chain (SHM_H) and light-chain (SHM_L) variable regions of the 28 clonotypes, arranged by clonal family (Fam.1–5) and singletons. SHM frequencies are expressed as the percentage divergence from the closest germline V allele. SHM was detected in both chains across the repertoire, ranging from 0% to 4.50% (heavy chain) and from 0% to 4.65% (light chain), with the highest heavy-chain frequency in singleton B7 (4.50%) and the highest light-chain frequencies in the clonally related functional clones E8 and D8 (4.65%). Colour intensity scales with mutation frequency as indicated. Values correspond to those listed in Supplementary Table 2.



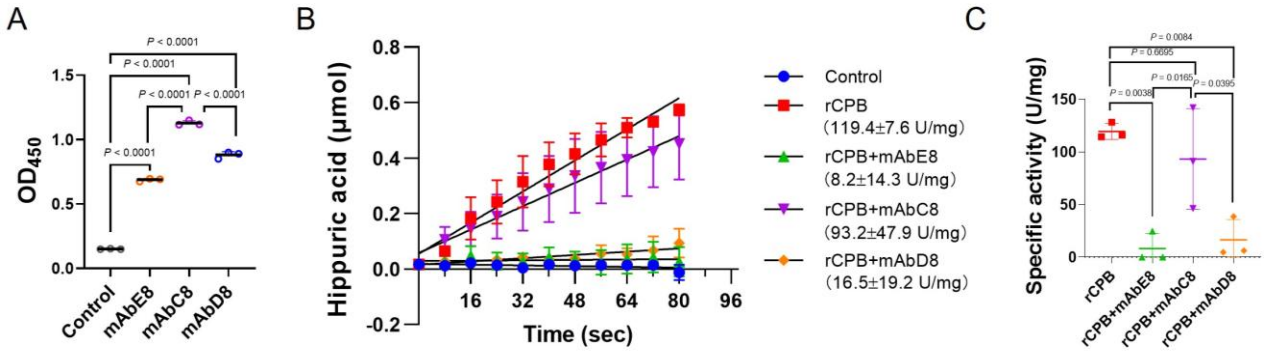
Supplementary Fig. 3. Vaccine-induced polyclonal CPB-specific antibody conferred mosquitocidal and transmission-blocking activity.

(A) Schematic of the membrane feeding assay (MFA): *A. stephensi* mosquitoes were fed on blood meals supplemented with purified CPB-pAb or control IgG. **(B)** CPB-pAb supplementation markedly increased mosquito mortality. Percent survival was monitored for 11 days; P value by log-rank (Mantel-Cox) test. **(C)** Oviposition was significantly reduced by CPB-pAb. Data are presented as mean ± SD with individual data points shown; Statistical significance was determined by two-tailed Student's t-test. **(D)** Schematic of the passive immunization and transmission-blocking assay: *Pb*-GFP-infected mice were passively transferred with CPB-pAb or control IgG before mosquito blood feeding. **(E)** Representative fluorescence microscopy images (10×) of *Pb*-GFP oocysts in mosquito midguts at 14 days post infection. BF, bright field. **(F)** Passive transfer of CPB-pAb significantly reduced oocyst counts per midgut. Data are presented as mean ± SD with individual data points shown; Statistical significance was determined by two-tailed Student's t-test. **(G)** The proportion of infected mosquitoes was significantly reduced in the CPB-pAb group. Proportions of infected (orange) and uninfected (grey) mosquitoes are shown; Fisher's exact test.



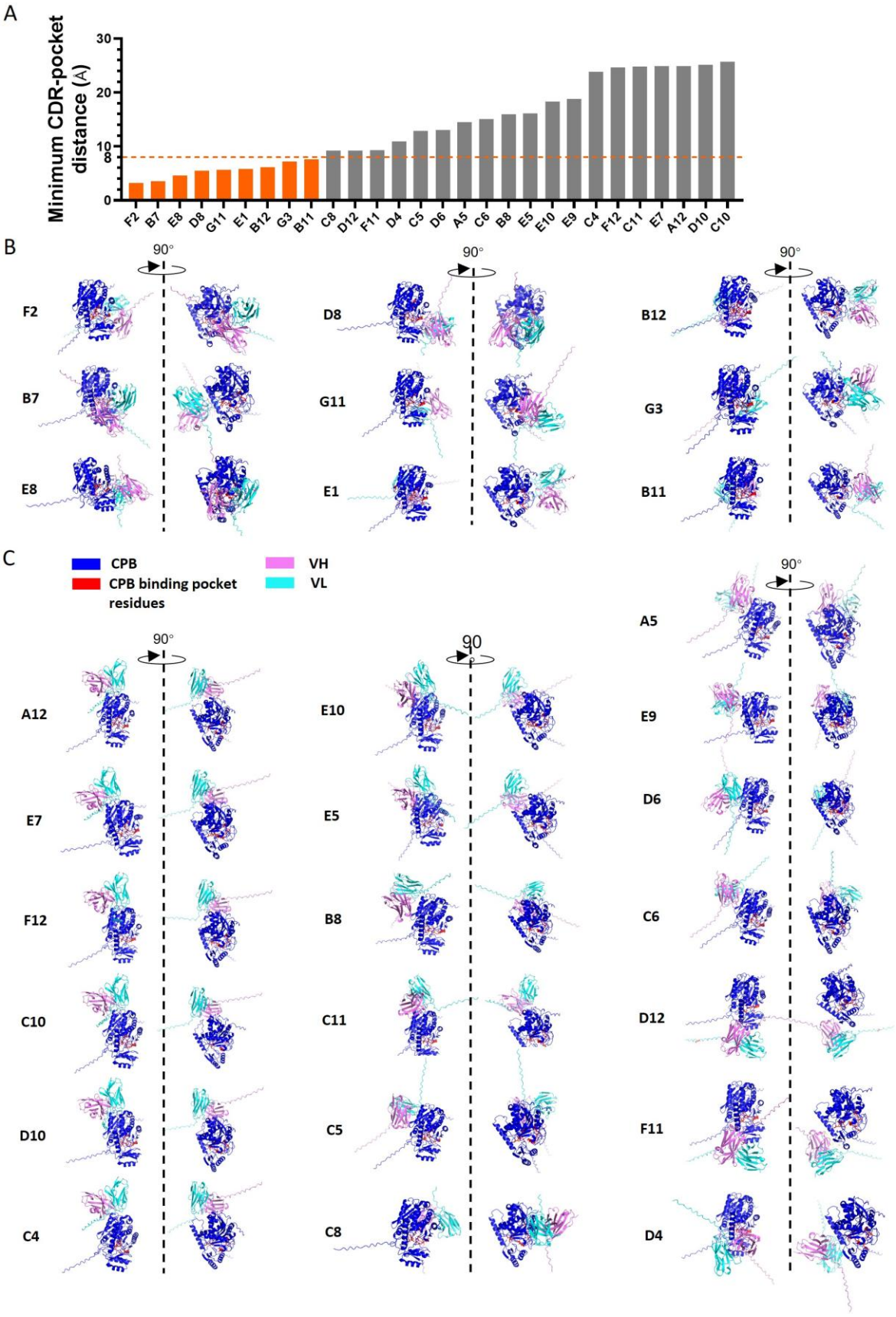
Supplementary Fig. 4. Cross-reactivity of vaccine-induced CPB-specific antibody against mosquito species.

CPB-pAb recognized CPB homologues in *Aedes aegypti*, *Anopheles sinensis* and *Culex pipiens pallens* by ELISA, whereas control IgG showed no reactivity.



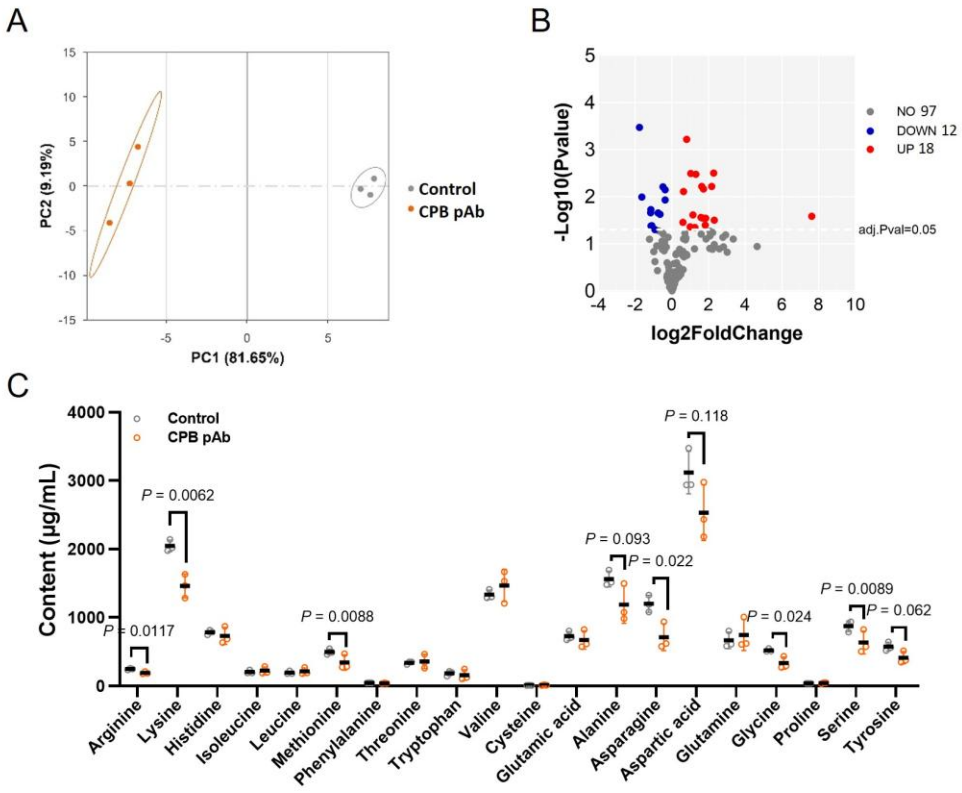
Supplementary Fig. 5. Functional CPB-specific mAbs inhibit CPB enzymatic activity despite comparable antigen binding.

(A) mAbE8, mAbC8 and mAbD8 bound CPB with comparable reactivity, whereas control IgG showed no detectable binding. Binding was analysed by ELISA; Data are presented as mean ± SD with individual data points shown; Kruskal-Wallis test with Dunn's multiple-comparisons test. **(B)** Preincubation with mAbE8 or mAbD8 profoundly reduced CPB-mediated hippuric acid production, whereas mAbC8 had minimal effect. Enzymatic activity was determined using hippuryl-L-arginine as substrate; Dots and error bars represent mean and SD of hippuric acid concentration at the indicated time points. **(C)** Specific activity of CPB was drastically reduced by mAbE8 (8.2 ± 14.3 U/mg, $P = 0.0038$) and mAbD8 (16.5 ± 19.2 U/mg, $P = 0.0084$) but not by mAbC8 (93.2 ± 47.9 U/mg, $P = 0.6695$), compared with CPB alone (119.4 ± 7.6 U/mg). Specific activity was calculated from the linear phase (0–80 s) of the kinetic curves in b; Data are presented as mean ± SD with individual data points shown (n = 3); Kruskal-Wallis test with multiple-comparisons.


A
Minimum CDR-pocket distance (Å)
30
20
10
8
0
F2 B7 E8 D8 G11 E1 B12 G3 B11 C8 D12 F11 D4 C5 D6 A5 C6 B8 E5 E10 E9 C4 F12 C11 E7 A12 D10 C10
B
90°
F2
B7
E8
D8
G11
E1
B12
G3
B11
C
CPB
CPB binding pocket residues
VH
VL
90°
A12
E7
F12
C10
D10
C4
E10
E5
B8
C11
C5
C8
A5
E9
D6
C6
D12
F11
D4

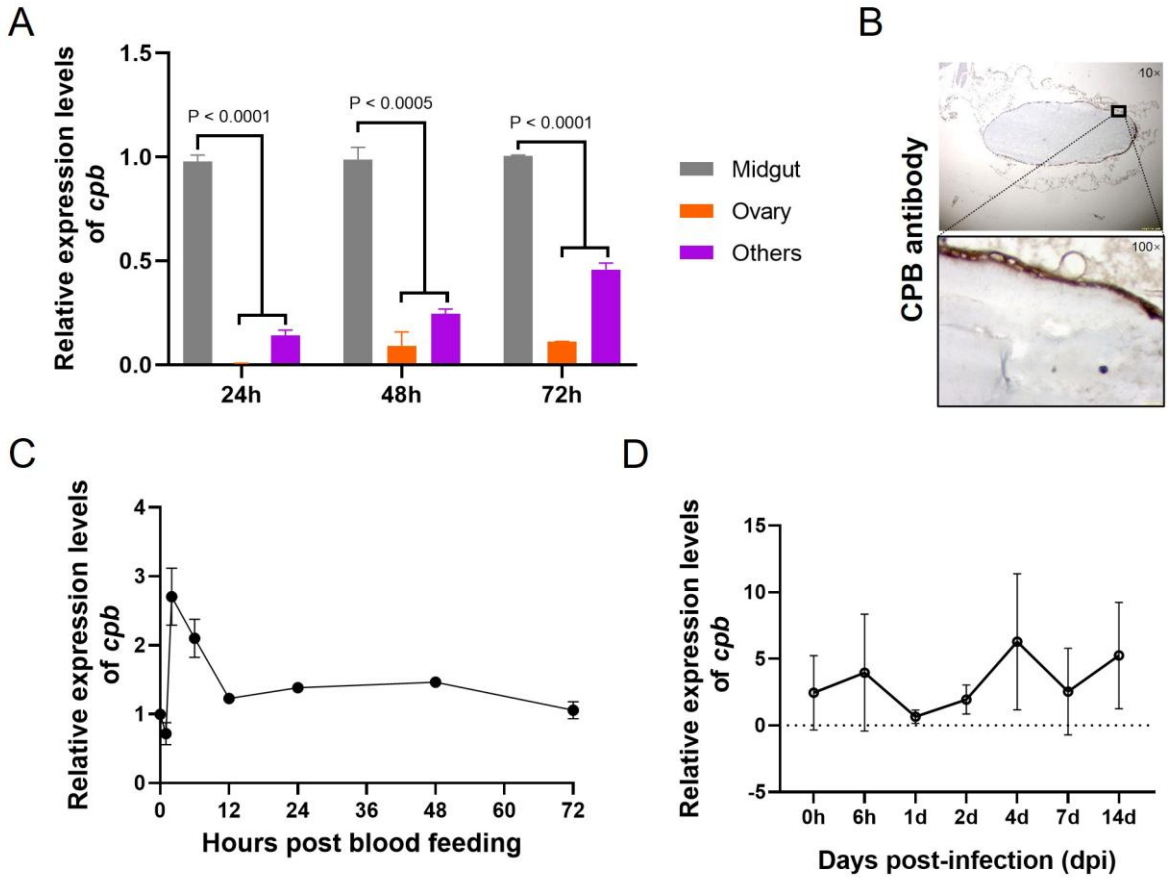
Supplementary Fig. 6. Epitope classification of all 28 clonotypes by AlphaFold3-predicted variable fragment-CPB complex structures.

For each of the 28 clonotypes, the variable fragment was modelled in complex with *A. stephensi* CPB using AlphaFold3, and the top-ranked model (highest ipTM) is shown in two orientations (90° rotation about the vertical axis). CPB is shown in blue, with active-site pocket residues in red; VH and VL are shown in magenta and cyan, respectively. **(A)** Nine clonotypes displayed a minimum CDR–pocket distance below the 8 Å contact threshold and were classified as active site-targeting (AST, orange); the remaining 19 were classified as non-AST (grey). Distances are sorted and the dashed line indicates the 8 Å cutoffs. **(B)** AST clonotypes position their paratopes at the rim or entrance of the CPB catalytic pocket, within interaction distance of the active-site core residues. **(C)** non-AST clonotypes engage distal surface regions of CPB remote from the catalytic pocket.



Supplementary Fig. 7. Targeted metabolomic analysis of amino acid profiles in CPB-specific antibody treated mosquito midguts.

(A) CPB-pAb treatment induced a profound shift in the midgut amino acid metabolome that clearly separated treated and control groups along PC1 (81.65% of variance; PERMANOVA, $P = 0.001$). PCA of targeted amino acid profiles in *A. stephensi* midguts at 24 h post blood meal. **(B)** Thirty of 127 targeted metabolites were differentially abundant (Benjamini-Hochberg-adjusted $P < 0.05$): 18 upregulated (red), 12 downregulated (blue) and 97 unchanged (grey). Volcano plot of targeted metabolites. **(C)** The canonical CPB substrates lysine ($P = 0.0062$) and arginine ($P = 0.0117$), together with methionine, asparagine, glycine and serine, were significantly reduced, indicating a specific defect in CPB-mediated terminal digestion rather than generalized impairment of amino acid absorption. Individual amino acid concentrations in mosquito midguts; Data are presented as mean ± SD with individual data points shown; Statistical significance was determined by two-tailed Student's t-test; Each replicate consisted of a pool of 30 mosquitoes, with three replicates per group.



Supplementary Fig. 8. Analysis of tissue-specific and temporal CPB expression patterns in *Anopheles stephensi*.

(A) CPB was expressed predominantly in the midgut relative to ovary and other tissues at 24-72 h post blood meal. Relative CPB transcript levels were determined by quantitative RT-PCR and normalized to rps7; Kruskal-Wallis test with Dunn's multiple-comparisons test. **(B)** Immunohistochemical staining confirmed that secreted CPB localizes to the interior side of the midgut epithelium. Top panel, 10×; bottom panel, 100× magnification of the boxed region. **(C)** *cpb* transcription was rapidly induced upon blood meal ingestion and declined thereafter. Relative expression was determined by quantitative RT-PCR at the indicated time points and normalized to rps7. **(D)** *cpb* transcription remained elevated in *Pb*-GFP infected mosquito midguts for up to 14 days post infection. Relative expression was determined by quantitative RT-PCR and normalized to rps7; Bars and error bars represent means and SD, respectively.

Supplementary Table 1. Primer sequence

Primers	5'-3' sequences	Species
CPB-F	CAGAACGTCCGCCGAATTAC	*Anopheles stephensi*
CPB-R	AAACCAAAGCCCTGATTGCG	
RPS7-F	ATCGCTATGGTGTTCGGTTC	
RPS7-R	TCCGAGTTCATTTCCAGCTC	
Pb18S-F	AAGCATTAAATAAAGCGAATACATCCTTAC	*Plasmodium berghei*
Pb18S-R	GGAGATTGGTTTTGACGTTTATGTG	

Supplementary Table 2. V(D)J gene usage and somatic hypermutation of single B cell clones

Type	SEQ ID	VH	DH	JH	CDR3H	SHM_H (%)	VL	CDR3L	SHM_L (%)
Fam.1	A12	IGHV1-62-2*01	—	IGHJ4*01	CARHENYAMDYW	0.7	IGKV10-96*01	CQQGNTLPWTF	1.4
	C11	IGHV1-62-2*01	—	IGHJ4*01	CARHENYAMDSW	0.7	IGKV10-96*01	CQQGNTLPWTF	1.4
	C10	IGHV1-62-2*01	—	IGHJ4*01	CARHENYAMDYW	0.7	IGKV10-96*01	CQQGNTLPLTF	1.4
	B8	IGHV1-62-2*01	—	IGHJ4*01	CARHENYAMDYW	0.0	IGKV10-96*01	CQQGNTLPWTF	1.4
	D10	IGHV1-62-2*01	—	IGHJ4*01	CARHENYAMDYW	0.7	IGKV10-96*01	CQQGYTLPWTF	1.4
	C4	IGHV1-62-2*01	—	IGHJ4*01	CARHENYAMDYW	0.7	IGKV10-96*01	CQQGNTLPWTF	1.4
	F12	IGHV1-62-2*01	—	IGHJ4*01	CARHENYAMDYW	1.0	IGKV10-96*01	CQQGKTLPWTF	2.5
	E7	IGHV1-62-2*01	—	IGHJ4*01	CARHENYAMDYW	0.7	IGKV10-96*01	CQQGYTLPWTF	1.8
	G11	IGHV1-62-2*01	—	IGHJ4*01	CARHENYAMDYW	1.7	IGKV10-96*01	CQQGNTLPWTF	2.5
Fam.2	A5	IGHV1-18*04	IGHD2-14*01	IGHJ2*01	CARRGRYDDYFDYW	1.4	IGKV3-7*02	CQHSWEIPYTF	0.0
	B12	IGHV1-18*04	IGHD2-14*01	IGHJ2*01	CARRGRYDDYFDYW	1.7	IGKV3-7*02	CQHSWEIPYTF	0.0
	F2	IGHV1-18*04	IGHD2-14*01	IGHJ2*01	CARRGRYDDYFDYW	1.4	IGKV3-7*02	CQHSWEIPYTF	0.3
	E1	IGHV1-18*04	IGHD2-14*01	IGHJ2*01	CARRGRYDDYFDYW	0.7	IGKV3-7*02	CQHSWEIPYTF	0.3
	B11	IGHV1-18*04	IGHD2-14*01	IGHJ2*01	CARRGKYDDYFDYW	2.0	IGKV10-96*01	CQQGNTLPWTF	1.4
Fam.3	E9	IGHV1-47-8*01	IGHD1-3*01	IGHJ2*01	CARKKDNFYFFGYW	0.7	IGKV14-111*01	CLQYDEFPYTF	2.5
	D12	IGHV1-47-8*01	IGHD1-3*01	IGHJ2*01	CARKKDNFYYFDYW	0.0	IGKV14-111*01	CLQYDEFPYTF	0.3
	F11	IGHV1-47-8*01	IGHD1-3*01	IGHJ2*01	CARKKDNFYYFDYW	0.7	IGKV14-111*01	CLQYADFPYTF	1.1
Fam.4	D6	IGHV8-4-15*01	IGHD4-1*01, IGHD4-1*02	IGHJ1*01	CARRRGNWDYWYFDVW	1.0	IGKV6-23*01	CQQYSSYLTF	1.4
	C6	IGHV8-4-15*01	IGHD4-1*01, IGHD4-1*02	IGHJ1*01	CARRRGNWGYWYFDVW	1.0	IGKV6-23*01	CQQYSSYLTF	0.7
Fam.5	E8	IGHV3-2-1*01	IGHD2-5*01, IGHD2-6*01	IGHJ2*01, IGHJ2*02	CARSSNYDFDYW	1.4	IGKV11-125*01	CLQHNSYPYTF	4.65
	D8	IGHV3-2-1*01	IGHD2-5*01, IGHD2-6*01	IGHJ2*01, IGHJ2*02	CARSSNYDFDYW	1.4	IGKV11-125*01	CLQHNSYPYTF	4.65
Singletons	D4	IGHV1-71-3*01	IGHD2-4*01, IGHD2-9*02	IGHJ3*01	CARGDYWFAYW	0.3	IGKV3-7*02	CQHSWEIPYTF	0.0
	C5	IGHV1-18-13*01	IGHD2-4*01, IGHD2-9*02	IGHJ4*01	CARRGYSDYDRDYYGMDYW	1.4	IGKV6-32*01	CQQDYSSPFTF	0.7
	E5	IGHV1-14*02	IGHD1-1*01	IGHJ2*01	CARDIYGSRGDHW	0.7	IGKV1-135*01	CWQGTHFPLTF	0.0
	G3	IGHV1-62-2*01	IGHD2-14*01	IGHJ3*01	CARHGYYRYDGPWFAYW	1.0	IGKV10-94*01	CQQYRKLPYTF	1.4
	B7	IGHV1-47-11*01	IGHD2-4*01, IGHD2-9*02	IGHJ4*01	CARGGIYYDYDGDAMDYW	4.5	IGKV3-12*01	CQHSRELPWTF	0.3
	E10	IGHV8-4-13*01	IGHD2-10*02, IGHD2-11*01, IGHD3-3*01	IGHJ3*01	CARIAPRTRFAYW	1.0	IGKV1-117*01	CFQGSHVPWTF	0.0
	C8	IGHV12-3*02	IGHD1-3*01	IGHJ2*01, IGHJ2*02	CASCIIGNFDYW	0.2	IGKV11-125*01	CLQHNSYPYTF	3.6

Supplementary Table 3. AlphaFold3-based epitope classification of the 28 CPB-specific clonotypes.

Clone	Min. CDR–pocket distance, heavy chain (Å)	Min. CDR–pocket distance, light chain (Å)	Min. CDR–pocket distance (Å)	Epitope classification
F2	3.2	9.73	3.2	AST
B7	7.86	3.56	3.56	AST
E8	4.63	6.96	4.63	AST
D8	5.48	10.9	5.48	AST
G11	5.76	5.66	5.66	AST
E1	5.78	11.71	5.78	AST
B12	6.17	11.45	6.17	AST
G3	7.51	7.21	7.21	AST
B11	7.62	8.22	7.62	AST
C8	9.2	15.57	9.2	non-AST
D12	9.21	17.25	9.21	non-AST
F11	9.35	17.86	9.35	non-AST
D4	10.94	16.87	10.94	non-AST
C5	12.91	19.46	12.91	non-AST
D6	13.03	17.35	13.03	non-AST
A5	14.51	17.18	14.51	non-AST
C6	15.04	22.91	15.04	non-AST
B8	15.96	26.47	15.96	non-AST
E5	16.09	23.75	16.09	non-AST
E10	18.34	22.49	18.34	non-AST
E9	18.81	19.68	18.81	non-AST
C4	24.72	23.84	23.84	non-AST
F12	26.02	24.62	24.62	non-AST
C11	25.67	24.81	24.81	non-AST
E7	24.86	26.05	24.86	non-AST
A12	25.92	24.88	24.88	non-AST
D10	25.22	25.11	25.11	non-AST
C10	25.74	27.21	25.74	non-AST